UNIVERSITY OF PORTSMOUTH

US AFSOR Study Report

The effects of LCF loadings on HCF crack growth

Annual Report for Phase II

F567

Submitted by:

R. F. Hall and B. E. Powell

May 1999

MECHANICAL BEHAVIOUR OF MATERIALS LABORATORY

DEPARTMENT OF MECHANICAL AND MANUFACTURING ENGINEERING

Anglesea Building, Anglesea Road
Portsmouth PO1 3DJ

Phone: +44 (0)1705 842332 +44 (0)1705 842325
E-mail: brian.powell@port.ac.uk rod.hall@port.ac.uk
Fax: +44 (0)1705 842351

REPORT DOCUMENTATION PAGE

Form Approved OMB No. 0704-0188

1. AGENCY USE ONLY (Leave blank)	2. REPORT DATE	3. REPORT TYPE AND DATES COVERED
	24 May 1999	Final Report

4. TITLE AND SUBTITLE

The Effects of LCF Loadings on HCF Crack Growth--Phase II

5. FUNDING NUMBERS

F61775-98-WE077

6. AUTHOR(S)

Professor Brian Powell

7. PERFORMING ORGANIZATION NAME(S) AND ADDRESS(ES)

University of Portsmouth
Anglesea Building
Anglesea Road
Portsmouth PO1 3DJ
United Kingdom

8. PERFORMING ORGANIZATION REPORT NUMBER

N/A

9. SPONSORING/MONITORING AGENCY NAME(S) AND ADDRESS(ES)

EOARD
PSC 802 BOX 14
FPO 09499-0200

10. SPONSORING/MONITORING AGENCY REPORT NUMBER

SPC 98-4056

11. SUPPLEMENTARY NOTES

12a. DISTRIBUTION/AVAILABILITY STATEMENT

Approved for public release; distribution is unlimited.

12b. DISTRIBUTION CODE

A

13. ABSTRACT (Maximum 200 words)

This report results from a contract tasking University of Portsmouth as follows: The contractor will investigate high cycle fatigue (HCF) effects in structural materials. This work will be a logical follow-on to a previous phase conducted under EOARD contract. In this phase, the contractor will begin by collating and reviewing all data relating to threshold values and combined high and low cycle fatigue testing on forged material previously developed at the contractor's laboratory. Following this step, the contractor will study the effects of different numbers and distributions on the LCF cycles on the crack growth rate for HCF loadings having a high stress ratio. Finally, the contractor will identify the jump-in (or step change) and implied (or derived) fatigue threshold values associated with these loadings and compare them with load shed values.

14. SUBJECT TERMS

EOARD, Materials, Structural Materials

15. NUMBER OF PAGES

42

16. PRICE CODE

N/A

17. SECURITY CLASSIFICATION OF REPORT	18. SECURITY CLASSIFICATION OF THIS PAGE	19. SECURITY CLASSIFICATION OF ABSTRACT	20. LIMITATION OF ABSTRACT
UNCLASSIFIED	UNCLASSIFIED	UNCLASSIFIED	UL

NSN 7540-01-280-5500

Standard Form 298 (Rev. 2-89)
Prescribed by ANSI Std. 239-18
298-102

UNIVERSITY OF PORTSMOUTH

US AFSOR Study Report

The effects of LCF loadings on HCF crack growth

Annual Report for Phase II

F567

Submitted by:

R. F. Hall and B. E. Powell

May 1999

MECHANICAL BEHAVIOUR OF MATERIALS LABORATORY

DEPARTMENT OF MECHANICAL AND MANUFACTURING ENGINEERING

Anglesea Building, Anglesea Road
Portsmouth PO1 3DJ
Phone: +44 (0)1705 842332 +44 (0)1705 842325
E-mail: brian.powell@port.ac.uk rod.hall@port.ac.uk
Fax: +44 (0)1705 842351

THE EFFECT OF LCF LOADINGS ON HCF CRACK GROWTH

REPORT FOR THE PERIOD 12 MAY 1998 - 11 MAY 1999

REPORT NO F 567

NOTATION

DCPD	direct current potential difference
FCG	fatigue crack growth
FOD	foreign object damage
HCF	high cycle fatigue
LCF	low cycle fatigue
MOC	multiple overload cycles: a type of HCF + LCF loading
MUC	multiple underload cycles: a type of HCF + LCF loading
SOC	single overload cycle: a type of HCF + LCF loading
SUC	single underload cycle: a type of HCF + LCF loading
da/dN_{HCF}	crack growth increment resulting from the application of a HCF cycle
da/dN_{LCF}	crack growth increment resulting from the application of a LCF cycle
da/dB	crack growth increment resulting from the application of a HCF + LCF loading block
da/dB_{HCF}	crack growth increment resulting from the application of the HCF cycles within a loading block
da/dB_{LCF}	crack growth increment resulting from the application of the LCF cycles within a loading block
ΔK, DK	stress intensity range
ΔK_{HCF}	stress intensity range associated with a HCF cycle
ΔK_{LCF}	stress intensity range associated with a LCF cycle, i.e. the peak-to-peak load cycle
ΔK_{onset}	the value of ΔK_{LCF} associated with the onset of HCF crack growth
ΔK_{th}	threshold value of stress intensity range
$K_{max,th}$	threshold value of maximum stress intensity
N_{HCF}	number of HCF cycles in a loading block
N_{LCF}	number of LCF cycles in a loading block
n	ratio N_{HCF} : N_{LCF}
R_{HCF}	stress ratio of the HCF cycles
R_{LCF}	stress ratio of the LCF cycles
T	overload ratio; i.e. the maximum LCF stress / maximum HCF stress.

1. INTRODUCTION

Continuing service failures in aero-engines and the increased use of ageing aircraft have highlighted the limitations in the current technical and fundamental understanding of the fatigue integrity of engineering components. There is at present

insufficient guidance to enable an engineer to account for the reduced high cycle fatigue (HCF) life consequent upon various forms and amounts of damage, such as low cycle fatigue (LCF), foreign object damage (FOD), corrosion, fretting etc., each of which promotes crack initiation, thereby compromising the HCF life. Thus it is that the US Secretary for Defence has declared that: "HCF is the number one readiness issue in the USAF". It is known for example that galling and fretting can reduce the HCF strength of titanium alloys by 80 and 60 % respectively. The two major concerns however are FOD and the complexity of the interactions between LCF and HCF. The second technical challenge is to incorporate non-destructive evaluation as an element of fatigue management. The concern here will always be to characterise the largest defect that is not detected in large structures and complex systems where inspectability may be difficult.

As a consequence, the present work is concerned to measure and model the fatigue crack growth rates associated with HCF loadings, particularly as they are affected by the presence of different proportions of LCF induced fatigue crack growth. The threshold values for HCF crack growth, both in the presence and absence of LCF crack growth, are studied, since they may be used to calculate critical crack sizes for components and structures subjected to HCF stress cycles.

2. EXPERIMENTAL DETAILS

The material selected for testing is Ti-6Al-4V. This is the most widely used titanium alloy, and it is extensively employed in the construction of aero-engine fans and compressors. All test pieces were cut from engine disc forgings that had been solution-treated and overaged. In this forged condition, the microstructure contained 47% primary alpha phase by volume, in the form of particles which were typically 45 μm long and 15 μm wide. The matrix of transformed beta consisted of colonies of aligned alpha separated by thin beta laminations, with an average colony width of 15 μm. Typical values of the room temperature tensile strength, proof stress and reduction in area exhibited by the material were 960 MPa, 860 MPa and 35%, respectively.

Corner notched testpieces having a 10 x 10 or 7 x 7 mm square cross-section at their gauge length have been cut from a Ti-6Al-4V disc. The specimen orientation, as defined by ASTM notation [**1**] was longitudinal - short transverse (LS) which corresponded to the growth of a crack through the thickness of a fan blade in response to centrifugally induced stresses.

The specimens have been cyclically loaded in a special test facility which combines an electromagnetic vibrator with a servohydraulic fatigue machine. This hybrid machine could therefore apply HCF cycles and LCF cycles either separately or conjointly. Figure **1** are a schematic representation of the four loading patterns used in the tests. The HCF cycles in these loading blocks are preceded by: a single underload cycle, multiple underload cycles, a single overload cycle, and multiple overload cycles. Consequently these loading blocks will be identified by the

abbreviations: SUC, MUC, SOC, and MOC, respectively. The HCF cycles were sinusoidal stress waves with a frequency of 157 Hz and a stress ratio of 0.8. The LCF cycles were trapezoidal stress waves with 1s rise and fall times and a stress ratio of 0.01. Table **1** records the stress levels and overload ratios (T) used in the tests. The overload ratio is given by the maximum LCF stress / maximum HCF stress.

Table 1 Stress levels and overload ratios

Type of test	Overload ratio (T)	LCF Stresses [MPa]		HCF Stresses [MPa]	
		Maximum	Minimum	Maximum	Minimum
SUC MUC	1.00	250	2.5	250	200
SOC MOC	1.15	287.5	2.5	250	200
SOC MOC	1.30	325	2.5	250	200
SOC MOC	1.45	362.5	2.5	250	200

The fatigue crack growth rates resulting from the repeated application of various combinations of HCF and LCF cycles have been measured with duplicate tests being undertaken for each loading pattern. Each specimen was precracked at room temperature in order to generate a near-quarter circular crack with a radius of not less than 0.6 mm. The final loads for the precracking were equal to, or less than, the loads to be used in testing. After the end of precracking, the length of the crack in the specimen was determined with the aid of acetate replicas. For testing, a pulsed direct current potential difference system (DCPD) was used to monitor the crack growth as a function of the number of applied cycles or loading blocks; the output of the system being the ratio of the voltage across the mouth of the crack to that across reference probes placed remotely but within the gauge length of the specimen. Each experiment was terminated at a crack length of approximately half the specimen width and, following the breaking open of the specimen, the final crack length was determined using an optical microscope.

The test data was analysed by the three-point secant method; the input data consisting of paired values of voltage ratio and either cycles or loading blocks corresponding to equal increments in the voltage ratio. This procedure resulted in a ratio of crack increment to crack length measuring precision of 20. The linear relationship between voltage ratio and crack length established by Hicks and Pickard [**2**], defined by the known values of voltage ratio and crack length measured at the start and end of the test, provided the calibration for the crack length monitoring system. The ranges of stress intensity factor associated with the HCF and LCF cycles were calculated using Pickard's [**3**] solution for the free surface position of a quarter-circular crack growing under remote tension.

In addition, the fatigue threshold values associated with a step-change from LCF to HCF loadings were determined. The crack was first grown at a stress ratio of 0.01, and then the HCF loading with a stress ratio of 0.8 was applied. The maximum applied LCF stress was equal to the maximum applied HCF stress, except where the effect of overload on ΔK_{th} was investigated, when the LCF stress was 1.3 times the maximum applied HCF stress.

Crack growth rates calculated on a small number of cycles are unreliable, so although the crack growth rate was monitored all through cycling, no data was stored until 1 million HCF cycles had been exceeded. Crack growth rates were then stored at frequent intervals up to 2 million HCF cycles. At 2 million HCF cycles the crack growth rate was tested in relation to the accepted threshold value of $1x10^{-8}$ mm/cycle. If the threshold value had not been exceeded, further LCF cycles at a stress ratio of 0.01 were applied to extend the crack and consequently increase ΔK, before returning to cycles at the same HCF loads as before. If the crack growth rate exceeded the accepted threshold value, the test was terminated.

During testing all crack lengths were estimated from the DCPD voltage ratio using data derived from previous tests. When the crack had extended half-way through, the specimen was broken open and the actual crack lengths measured. Using these lengths, corrections were then made to the stored values of FCG rates and of ΔK. The corrected data was inspected for FCG rates of $1x10^{-8}$ mm/cycle and the spread of ΔK over which these occurred have been quoted as the range of ΔK_{th}. Low crack growth rates, those below $1x10^{-9}$ mm/cycle, were eliminated and charts of near-threshold FCG rates constructed.

This new procedure for the determination of fatigue threshold values replaced the previous old method in which the sampling of the HCF crack growth rate was restricted to the application of only 500 000 HCF cycles.

3 RESULTS

3.1 HCF and LCF applied separately

The fatigue threshold value and the near-threshold FCG rates have been determined for $R_{HCF} = 0.8$ using the jump-in, or step change, method. Figure **3** compares the results of the old and new methods of sampling and analysing the threshold test data. The new method yields more growth rate data, a more accurate threshold value, and gives greater confidence in the result.

Two load sequences [Figure **2**] having overload ratios of 1.00 and 1.30, were used in the jump-in tests. The threshold values determined by the new method are presented in Table **2** and the associated FCG rate data are shown in Figure **4**. Given the accuracy with which threshold values can be determined there appears to be no

significant difference in the results for T = 1.00 and 1.30. The mean value is 2.9 MPa$\sqrt{m}$.

Table 2. Threshold values corresponding to a FCG rate of $1x10^{-8}$ mm/cycle determined by the jump-in method

Specimen No	Overload ratio [T]	Threshold value [MPa$\sqrt{m}$]
2014	1.00	2.7 - 2.8
2042	1.00	2.9 - 3.1
2042	1.30	3.0 - 3.2
2041	1.30	2.6 - 2.8

Following the determination of the fatigue threshold value using jump-in tests at T = 1.00, the crack was allowed to grow under the application of HCF cycles only and the near-threshold FCG rates were determined. The results, presented in Figure **5,** show that the data from duplicate tests are generally in agreement. The line representing a second order polynomial equation has been visually fitted through the data which extrapolates to a threshold stress intensity range of 2.9 MPa$\sqrt{m}$ at da/dN = $1x10^{-8}$ mm/cycle.

The fatigue crack growth rate results from tests using solely LCF cycles are presented in Figure **6**. Again there is good correlation between the data from the duplicate tests. This gave greater confidence in the fitting of straight lines through the plot. Previous work [**4**] has demonstrated that within the Paris regime Ti-6Al-4V has a bi-linear FCG rate response to LCF loadings. A similar response from the current tests is evident from the data in Figure **6**, with a point of inflection, or intersection, at 17.5 MPa$\sqrt{m}$. The two lines constructed through the results are used in subsequent diagrams to represent the LCF component of combined HCF+LCF data and in the linear summation predictions of the FCG rates developed by such loadings.

3.2 Single underloads

Results from HCF+LCF cycle tests with SUC loading blocks are presented as Figure **7**. Apart from an initial variation in growth rate at the lower values of ΔK_{LCF}, there is a good agreement between the test data. A second order polynomial fit has been constructed through the test data, which intersects the LCF straight lines established in Figure **6**. The stress intensity range at which the polynomial intersects the straight lines can be considered as the point at which the growth due to the HCF cycles

begins to contribute to crack growth in response to the application of the loading blocks. This intersection occurs at $\Delta K_{LCF} = 12.6$ MPa$\sqrt{m}$, which equates to a value of $\Delta K_{HCF} = 2.5$ MPa$\sqrt{m}$, since:

$$\Delta K_{HCF} = \Delta K_{LCF} (\Delta\sigma_{HCF}/\Delta\sigma_{LCF}) \qquad \text{--------(4.1)}$$

and thus:

$$\Delta K_{HCF} = \Delta K_{LCF} (1 - R_{HCF}) / (1 - R_{LCF}) \qquad \text{-------(4.2)}$$

In the absence of any crack growth acceleration or retardation due to load interaction effect, the linear summation model is expected to predict the FCG rates for HCF + LCF loadings. These predictions are given by the relationship:

$$da/dB = N_{HCF} \times da/dN_{HCF} + N_{LCF} \times da/dN_{LCF} \qquad \text{-------(4.3)}$$

The relationship between da/dN_{HCF} and ΔK_{HCF} represented by the polynomial equation fitted to the HCF test data in Figure **5**, and the relationship between da/dN_{LCF} and ΔK_{LCF} given by the equations for the straight lines in Figure **6**, may be use to generate a linear summation prediction of the FCG rates for the HCF+LCF cycle tests with SUC loading blocks. Figure **8** compares the experimental and predicted FCG rates, plotted as a function of the stress intensity ranges ΔK_{HCF}. It is readily apparent that the prediction gives slightly conservative values of FCG rates in relation to the test data, for $\Delta K_{HCF} > 3.0$ MPa$\sqrt{m}$. Thus any lifing estimates using these predictions would err positively, but not greatly, on the side of safety.

3.2 Multiple underloads

Fatigue crack growth rates developed as the result of the application of HCF + LCF loading patterns involving multiple underloads have been determined. The results for MUC loading blocks containing 1000 HCF cycles to 10 LCF cycles are presented as Figure **9**. There is considerable specimen-to-specimen variation in the data generated by these three tests. Consequently, a polynomial fit has been constructed through the data from the test which produced the mean FCG rates. This polynomial intersects the straight lines representing the LCF data at $\Delta K_{LCF} = 12.9$ MPa$\sqrt{m}$, which corresponds to a value of $\Delta K_{HCF} = 2.6$ MPa$\sqrt{m}$. The results for a single test using MUC loading blocks containing 10 000 HCF cycles to 10 LCF cycles are presented as Figure **10**. The polynomial fit to this data intersects the straight lines representing the LCF data at $\Delta K_{LCF} = 12.0$ MPa$\sqrt{m}$, which corresponds to a value of $\Delta K_{HCF} = 2.4$ MPa$\sqrt{m}$.

The crack growth response to single and multiple underload cycles have been compared using SUC loading blocks with a ratio of 1000 HCF cycles to 1 LCF cycle and MUC loading blocks of 1000 HCF cycles to 10 LCF cycles. Figure **11** shows that the effect of increasing the number of LCF cycles in the loading blocks is to increase the HCF + LCF growth rate (da/dB) and to reduce its separation from that for the LCF cycles (da/dB_{LCF}). Thus the crack growth behaviour corresponds to the pattern of changes indicated by the sequence of linear summation model prediction given in Figure **12**.

The applicability of the linear summation model to the results of the MUC tests is considered next. Figure **13** compares the experimental and predicted FCG rates for the application of MUC loading blocks with a cycle ratio of 1000:10, plotted as a function of the stress intensity ranges ΔK_{HCF}. There is a good agreement between the linear summation predictions and the experimental results of test CN2020, and poor agreement for the other test results. In the case of the test employing loading blocks with cycle ratios of 10 000:10 the agreement between the measured and predicted growth rates is again poor (Figure **14**). For the greater part the model predictions fail at the lower values of ΔK_{HCF}, notably for $\Delta K_{HCF} < 3.0$ MPa$\sqrt{m}$.

Compared to the SUC loading block of 1000:1, the MUC loading block of 10 000 :10 contains 10 times the number of HCF cycles and 10 times the number of LCF cycles. The linear summation model would therefore predict that the FCG rates for the MUC loading would be 10-times that for the SUC loading. The comparison given in Figure **15** shows that, apart for the lower values of ΔK, this is indeed the case.

3.4 Single overloads

A sequence of tests have used loading blocks with a single initial LCF overload cycle to elucidate the effect of its size on the subsequent HCF crack growth within the block. Overload ratios [T] of 1.00, 1.15, 1.30 and 1.45 have been used, where the overload ratio is given by the maximum LCF stress / maximum HCF stress. Table **1** gives the stresses used in the tests, a cycle ratio of 1000:1 being employed throughout. It should be noted that SOC tests are those in which the HCF cycles are actually preceded by an underload - overload sequence, and thus a T value of 1.00 corresponds to a SUC test.

What is the best way to present a set of FCG rate results in which the ratio of ΔK_{LCF} : ΔK_{HCF} is changed? A plot of da/dB versus ΔK_{LCF} is a form of presentation which has been extensively used in the past to summarise the results of HCF/LCF tests. Figure **16** shows the plots of da/dB versus ΔK_{LCF} for the four overload ratios studied in which the polynomial fits to the post-onset crack growth test data are presented. Figure **17**, which compares these four polynomial fits to the LCF only data, suggests to the reader that increasing T has the effect of progressively reducing da/dB whilst delaying the onset of HCF crack growth. Such crack growth retardation due to the

application of overloads is a reasonable expectation. However, these effects are overstated because increasing the value of T increases the ratio ΔK_{LCF} : ΔK_{HCF}, as Table **1** infers. Table **3** gives the FGC rate at a cycle ratio of 1000:1 and at ΔK_{LCF} = 25 MPa$\sqrt{m}$ for each of these overload ratios. But the effect of T is more correctly seen when the values of da/dB are compared at a fixed value of ΔK_{HCF}.

Table 3. FCG rates for SUC and SOC loadings at ΔK_{LCF} = 25 MPa$\sqrt{m}$ and ΔK_{HCF} = 5.05 MPa$\sqrt{m}$

Overload ratio [T]	FCG Rate, da/dB [mm/block]	
	ΔK_{LCF} = 25	ΔK_{HCF} = 5.05
1.00	2.6×10^{-3}	2.6×10^{-3}
1.15	8.9×10^{-4}	1.3×10^{-3}
1.30	5.6×10^{-4}	1.4×10^{-3}
1.45	4.5×10^{-4}	1.5×10^{-3}

Table **4**. shows that when a value of ΔK_{HCF} corresponding to the onset of HCF crack growth is calculated using equation **4.1** that there is in fact no delay in onset resulting from an increase in T within the range studied The value of ΔK_{HCF} corresponding to the onset of HCF crack growth derived from this data is in the range 2.3 - 2.6 MPa$\sqrt{m}$, a value similar to or less than the threshold values determined in the relevant jump-in tests.

Table 4. The effect of overload ratio on the onset of HCF crack growth

Overload ratio [T]	ΔK_{LCF} [MPa$\sqrt{m}$]	ΔK_{HCF} [MPa$\sqrt{m}$]
1.00	12.6	2.6
1.15	12.9	2.3
1.30	14.5	2.3
1.45	17.9	2.5

The effects of LCF loading on HCF crack growth are better presented as plots of da/dB versus ΔK_{HCF} [Figure **18**]. This shows similar curves for the SOC tests [T=1.15, 1.30, 1.45], particularly at the faster FCG rates, which are different to those for the SUC test condition [T=1.00]. The figure indicates the change in total FCG rate with increasing T for values of ΔK_{HCF}, the general effect being to rotate the FCG rate curve in a anticlockwise manner about a turning point approximately located at ΔK_{HCF} =

2.9 MPa$\sqrt{m}$ and da/dB = 2.2 x 10^{-4} mm/cycle.

3.5 Multiple overloads

Fatigue crack growth rates developed as the result of the application of HCF + LCF loading patterns involving multiple overloads have been determined. The results for MOC loading blocks containing 1000 HCF cycles to 10 LCF cycles are presented as Figure **19**. A polynomial fit to the data intersects the straight lines representing the LCF data at ΔK_{LCF} = 11.8 MPa$\sqrt{m}$, which corresponds to a value of ΔK_{HCF} = 1.8 MPa$\sqrt{m}$.

The crack growth response to single and multiple overload cycles has been compared using SOC loading blocks with a ratio of 1000 HCF cycles to 1 LCF cycle and MOC loading blocks of 1000 HCF cycles to 10 LCF cycles. The data are for T=1.30, and in each case the measured FCG rates are compared with the crack growth rates for the LCF component of the loading (Figure **20**). The proximity of the growth rate curves for HCF + LCF and the LCF component of each loading again increases as the number of LCF cycles in the loading block increases.

The crack growth response to multiple underload cycles (T=1.00) and multiple overload cycles (T=1.30) have been determined using loading blocks with a ratio of 1000 HCF cycles to 10 LCF cycles. These data, presented in Figure **21**, show that increasing the overload ration also increases the proximity of the growth rate curves for HCF + LCF and the LCF component of each loading. A comparison of the FCG rate curves for MUC and MOC loading, plotted as a function of ΔK_{HCF}, (Figure **22**) suggests that the effect of the overloads is to shift the FCG curve to lower values of ΔK_{HCF}.

4. DISCUSSION

The predictions of the linear summation model suggested that the introduction of a greater number of LCF cycles into each loading block, and the use of LCF cycles developing overloads rather than underloads, would both reduce the significance of the HCF crack growth. The FCG rate curve for the HCF + LCF loading would move closer to that for the LCF only loading as a result of these modifications to the loading blocks. Both expectations are realised. First, the influence of the number of LCF cycles is demonstrated clearly in the comparison of the SUC and MUC results (Figure **11**), and is also evident in the comparison of the SOC and MOC test results (Figure **20**). Second, the expected effect of overloads in comparison to underloads is clearly shown in Figure **17**, and is evident in Figure **21**.

However there are expectations which are not realised. For example, the fatigue threshold values measured in the jump-in tests do not correspond to the values for the onset of HCF crack growth in the HCF + LCF tests. The threshold values for HCF

cycles at R_{HCF} = 0.8, obtained from the jump-in tests, for both T = 1.00 and 1.30, are in the range 2.7 - 3.2 MPa$\sqrt{m}$, the average value being 2.9 MPa$\sqrt{m}$. The threshold values obtained by construction, that is the intersection of the polynomial representing the HCF + LCF data and the straight lines representing the LCF data are, with one exception, in the range 2.3 - 2.7 MPa$\sqrt{m}$ (Table **5**). An even lower value is obtained for the MOC test, but the application of multiple overloads produces the FCG rate curve which is the closest to the LCF only lines (Figure **19**) and this is the condition for the least accurate determination of the onset value for HCF crack growth.

Table 5. Conditions corresponding to the onset of HCF crack growth

Test type	Overload ratio [T]	ΔK_{LCF} [MPa$\sqrt{m}$]	ΔK_{HCF} [MPa$\sqrt{m}$]
SUC 1000:1	1.00	12.6	2.5
MUC 1000:10	1.00	12.9	2.6
MUC 10 000:10	1.00	12.0	2.4
SOC 1000:1	1.15	12.9	2.3
SOC 1000:1	1.30	14.5	2.3
SOC 1000:1	1.45	17.9	2.5
MOC 1000:10	1.30	11.8	1.8

The threshold value recorded in this study are similar to or higher that those indicated by others. A previous study [**6**] measured the fatigue threshold of forged Ti-6Al-4V at R_{HCF} = 0.82 to be 2.2 MPa$\sqrt{m}$ when using the load shedding method; and calculated the onset of HCF crack growth from HCF + LCF tests to be 2.3 MPa$\sqrt{m}$. The load shed fatigue threshold value for forged Ti-6Al-4V in the solution treated and overaged condition estimated from the work of Hopkins et al [**7**] is approximately 2.3 MPa$\sqrt{m}$ at R = 0.8. Estimates from the work of Marci et al [**8**] who used the jump-in test method on solution treated and aged Ti-6Al-4V plate material, suggest a threshold value in the range 2.25 - 2.5 MPa$\sqrt{m}$, with the same value for T = 1.0 and T = 1.3.

The general expectations that overloads would increase threshold values relative to those for the application of underloads was not realised; neither in the jump-in tests, nor in the values for the onset of HCF crack growth in HCF + LCF tests. For the size of overloads and underloads studied the threshold values were not significantly different, whilst the apparent rotation (Figure **18**) or shift (Figure **22**) of the FCG rate curves consequent upon the application of overload cycles would suggest that if anything overloads favour a reduction in the HCF threshold value.

Yang [**9**] found that an underload - overload sequence had a negligible delaying effect on crack growth in the creep resistant titanium alloy IMI 834 at T= 1.25, although this

observation is for R_{HCF} = 0.3 only. The stress ratio of the HCF cycles is important since Tsukuda et al [**10**] noted that the transient crack growth behaviour following a single overload in 2017-T3 aluminium alloy at high R ratios [i.e. 0.7] was significantly different to that at low R ratios [i.e. 0]. At high stress ratios the initial retardation is followed by an acceleration, but the acceleration phase does not occur at low stress ratios.

If Figures **7**, **9** and **10** are examined it is seen that for some tests the FCG rates prior to the onset of HCF crack growth are noticeably faster than those indicated by the dotted line which represents the mean of the LCF only data. In the case of these three figures, there is evidently a specimen-to-specimen variation, the effect being seen in the faster FCG rates initially developed in 4 of 6 tests. Similar behaviour has been seen in other studies of HCF + LCF crack growth behaviour in Ti-6Al-4V in the forged [**11**] and cross-rolled [**12**] conditions.

As Figure **6** shows there is scatter in the LCF data below 17.5 MPa$\sqrt{m}$. This scatter is effectively encompassed by a band giving a two-fold variation in FCG rate at any given value of ΔK_{LCF}. Figures **23** and **24** plot the HCF + LCF crack growth rates for $\Delta K_{LCF} < 17.5$ relative to such a scatter band. The data that lie above this scatter band may be considered to be examples of the "pre-onset enhancement" of crack growth rates. Examination of Figures **23** and **24** shows that "pre-onset enhancement" is more frequently associated with the tests involving underloads [open symbols] rather than with tests involving overloads [closed symbols].

The contribution of the HCF cycles to the observed growth under HCF + LCF loading blocks can be estimated on the assumptions that the growth associated with each applied HCF cycle in any block is the same, and that any load interaction effect will result in the LCF crack growth modifying the HCF crack growth rather than the converse. On this basis the HCF crack growth rates can be calculated from the HCF + LCF test data using the relationship:

$$da/dN_{HCF} = (da/dB - N_{LCF} * da/dN_{LCF}) / N_{HCF} \qquad \text{-----(4.4)}$$

Figure **25** gives the calculated HCF crack growth rates, da/dN_{HCF}, plotted against ΔK_{HCF} for SUC and SOC tests. The effect of overloads appears to be a reduction in the threshold value, and a reduction in the FCG rates at $\Delta K_{HCF} > 3.0$ MPa$\sqrt{m}$. Figure **26** compares the calculated near threshold HCF crack growth data for T= 1.00 with those determined from jump-in threshold tests. The threshold values derived from the HCF + LCF tests appears to be lower. Figure **27** compares the calculated HCF crack growth rate curves for MUC and MOC tests. In this case the effect of overloads appears to be a reduction in the threshold value and similar growth rates for ΔK_{HCF} > 3.0 MPa$\sqrt{m}$.

The cusps in the calulated FCG rate curves (Figures **25** and **27**) are the result of adopting a bi-linear representation of the LCF data. Clearly a polynomial representation of the LCF data is to be preferred for this application.

Future work includes the re-examination of the calculated FCG rates, and the development of the model for predicting the FCG rates generated by SOC and MOC tests.

5.CONCLUSIONS

Fatigue crack growth rates have been measured in Ti-6Al-4V at room temperature. HCF loadings with a stress ratio of 0.8 and LCF loadings with a stress ratio of 0.01 have been applied, both separately and in various combinations.

The crack growth rate data resulting from the application of a separate LCF loadings are bi-linear within the Paris regime, whilst the HCF near-threshold crack growth data extrapolate to a fatigue threshold value of 2.9 MPa$\sqrt{m}$. These data form the basis of the linear summation predictions.

The jump-in threshold values determined both with and without an overload of 30 % are similar, and are in the range 2.9 ± 0.3 MPa$\sqrt{m}$.

For tests involving SUC and MUC loading blocks, the threshold value for the onset of HCF crack growth found by construction are in the range 2.3 - 2.6 MPa$\sqrt{m}$. The linear summation model generally gives a fair representation of the crack growth data, but there are examples of enhanced HCF + LCF crack growth prior to the predicted threshold value [2.9 MPa$\sqrt{m}$]. The growth rates with 10 000 LCF cycles to 10 LCF cycles is 10-times that for 1000 HCF cycles to 1 LCF cycle, but enhanced HCF + LCF crack growth below 2.9 MPa$\sqrt{m}$ is again observed.

Introducing a single overload into each loading block appears to rotate the FCG rate curve, thereby increasing the crack growth rates for $\Delta K_{HCF} < 2.9$ MPa$\sqrt{m}$. and decreasing them for $\Delta K_{HCF} > 2.9$ MPa$\sqrt{m}$. The HCF + LCF crack growth rates for overload ratios of 1.15. 1.30 and 1.45 are similar when plotted as a function of ΔK_{HCF}.

A comparison of the SUC and MUC test results, and a comparison of the SOC and MOC test results, show that increasing the number of LCF cycles in the loading blocks shifts the HCF + LCF crack growth curve to faster rates and brings it closer to that expected for LCF cycles alone.

A comparison of MUC and MOC test results suggests the introduction of overloads shifts the FCG rate curve to lower values of ΔK_{HCF}.

REFERENCES

1 ASTM Standard E-399-90, 1990, *03.01*, 407

2 Hicks, M. A. and Pickard, A. C. *Int. J. of Fract.* 1980, *20*, 91

3 Pickard, A. C. *The Application of 3-Dimensional Finite Element Methods to*

Fracture Mechanics and Fatigue Life Predictions EMAS, Warley, UK.1986
4 Powell, B. E., Hawkyard, M. and Grabowski, L. *Int. J. Fatigue*, 1997, *19,* Supp. 1, S167
5 Powell, B. E. and Duggan, T. V. *Int. J. Fatigue*. 1987, *9,* 195
6 Powell, B. E. "The influence of minor cycles on low cycle fatigue crack propagation", *PhD Thesis*, University of Portsmouth 1985.
7 Hopkins, S. W. Rau, C. A. Leverant, G. R. and Yuen, A. "Effects of various programmed overloads on the threshold for high-frequency fatigue crack growth. "*ASTM STP 595,* 1976, 125
8 Marci, G. Castro. D. E. and Bachmann, V. "Fatigue crack propagation threshold", *J. Testing and Evaluation,* 1989, *17*, 28
9 Yang, R. "Prediction of crack growth under complex loading cycles", *Int. J. Fatigue,* 1994, *16,* 397
10 Tsukuda H. Ogiyama, H. Shiraishi, T. "Transient fatigue crack growth behaviour following single overloads at high stress ratios", *Fatigue and Fracture of Engineering Materials and Structures,* 1996, *19*, 879
11 Hawkyard, M. Powell, B. E. Hussey, I. and Grabowski, L. "Fatigue crack growth under the conjoint action of major and minor stress cycles", *Fatigue and Fracture of Engineering Materials and Structures,* 1996, *19,* 217
12 Hawkyard, M. Powell, B. E. and Grabowski, L. "The growth of cracks in Ti-6Al-4V plate material under combined high and low cycle fatigue", *Int. J. Fatigue,* 1997, *19,* S167

FIGURES

Figure 1 Schematic representation of the repeated stress - time sequences used in the tests considered in this report. a) Single Underload Cycle; b) Multiple Underload Cycle; c) Single Overload Cycle; d) Multiple Overload Cycle.

Figure 2 Schematic representation of the stress - time sequences used in the jump-in threshold tests. a) Overload ratio, (T) = 1.0; b) Overload ratio, (T) = 1.3.

Figure 3 Comparison of methods used to represent the determination of ΔK_{th}. Data for jump-in tests at T=1.0. a) Old method; b) New method.

Figure 4 Comparison of FCG rates around threshold between tests at: a) T=1.0; b) T=1.3.

Figure 5 Near-threshold FCG rates with a visual polynomial fit through the mean of the data extrapolated to an FCG rate of 10^{-8}mm/cycle. Test data for T=1.0

Figure 6 A bi-linear fit through the LCF only test data. The lines are used to represent LCF test data in subsequent charts. Test data for duplicate tests at R_{LCF}=0.01

Figure 7 A polynomial fit through the FCG data for SUC tests. Test data for duplicate tests at: T=1.0; n=1000:1.

Figure 8 Comparison of predicted and experimental FCG rates for SUC tests. Test data for duplicate tests at n=1000:1.

Figure 9 A polynomial fit through the FCG data for MUC tests. Test data for three tests at: T=1.0; n=1000:10.

Figure 10 A polynomial fit through the FCG data for MUC test. Test data for a single test at: T=1.0; n=10 000:10.

Figure 11 Comparison of FCG rates for SUC and MUC tests. Data for: T=1.0; n=1000:1 and n=1000:10.

Figure 12 The predicted effect of cycle ratio on the LCF+HCF and LCF only crack growth rates. Data for: a) n=10 000:1; b) n=10 000:10; c) n=10 000:100; d) n=10 000:1000.

Figure 13 Comparison of predicted and experimental FCG rates for MUC tests. Test data for duplicate tests at n=1000:10.

Figue 14 Comparison of predicted and experimental FCG rates for MUC tests. Test data for: T=1.0; n=1000:10 and n=10 000:10.

Figure 15 Comparison of FCG rate data for: a MUC test at 10 000:10; 10-times the SUC test data at 1000:1, and 10-times the LCF only test data.

Figure 16 Polynomial fits through the FCG data for LCF+HCF tests at different overload ratios. Test data for duplicate tests with n=1000:1 at: a) T=1.0; b) T=1.15; c) T=1.3; d) T=1.45.

Figure 17 Comparison of the polynomial fits from Figure 16 with the LCF only test data, plotted as a factor of ΔK_{LCF}. Test data for n=1000:1.

Figure 18 Comparison of the polynomial fits from Figure 16, plotted as a function of ΔK_{HCF}. Test data for n=1000:1.

Figure 19 A polynomial fit through FCG data for MOC tests. Data for duplicate tests at: n=1000:10; T=1.3

Figure 20 Comparison of FCG rates for SOC and MOC tests. Data for T=1.3 at

n=1000:1 and n=1000:10.

Figure 21 Comparison of FCG rates for MUC and MOC tests. Data for n=1000:10 at T=1.0 and T=1.3.

Figure 22 Comparison of the polynomial fits from MUC and MOC data, plotted as a function of ΔK_{HCF}. Test data for n=1000:10 at T=1.0 and T=1.3.

Figure 23 FCG rates for SUC and SOC test loadings relative to a LCF scatterband of times 2. Data for n=1000:1.

Figure 24 FCG rates for MUC and MOC test loadings relative to a LCF scatterband of times 2. Data for n=1000:10.

Figure 25 HCF crack growth rates calculated from SUC and SOC test data shown in Figure 16. Data for n=1000:1.

Figure 26 Comparison of the experimental and calculated HCF crack growth rates. Test data for T=1.0.

Figure 27 HCF crack growth rates calculated from MUC and MOC test data shown in Figures 9 and 19. Data for n=1000:10

[Documents F567-d1.doc & F567-d2.doc &F567bu.doc / 12 May 1999 / issue 8]

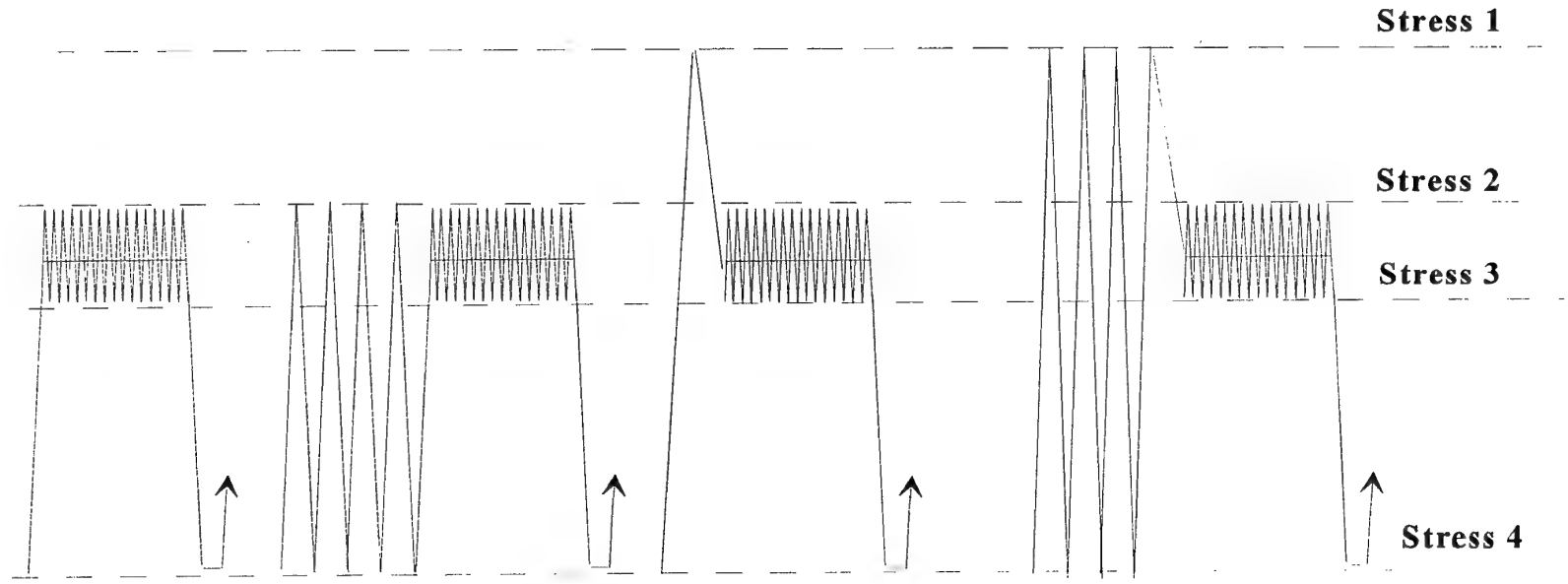

Figure 1 **Schematic representation of the repeated stress - time sequences used in the tests considered in this report. (a) Single Underload Cycle; b) Multiple Underload Cycles (c) Single Overload Cycle; (d) Multiple Overload Cycles.**

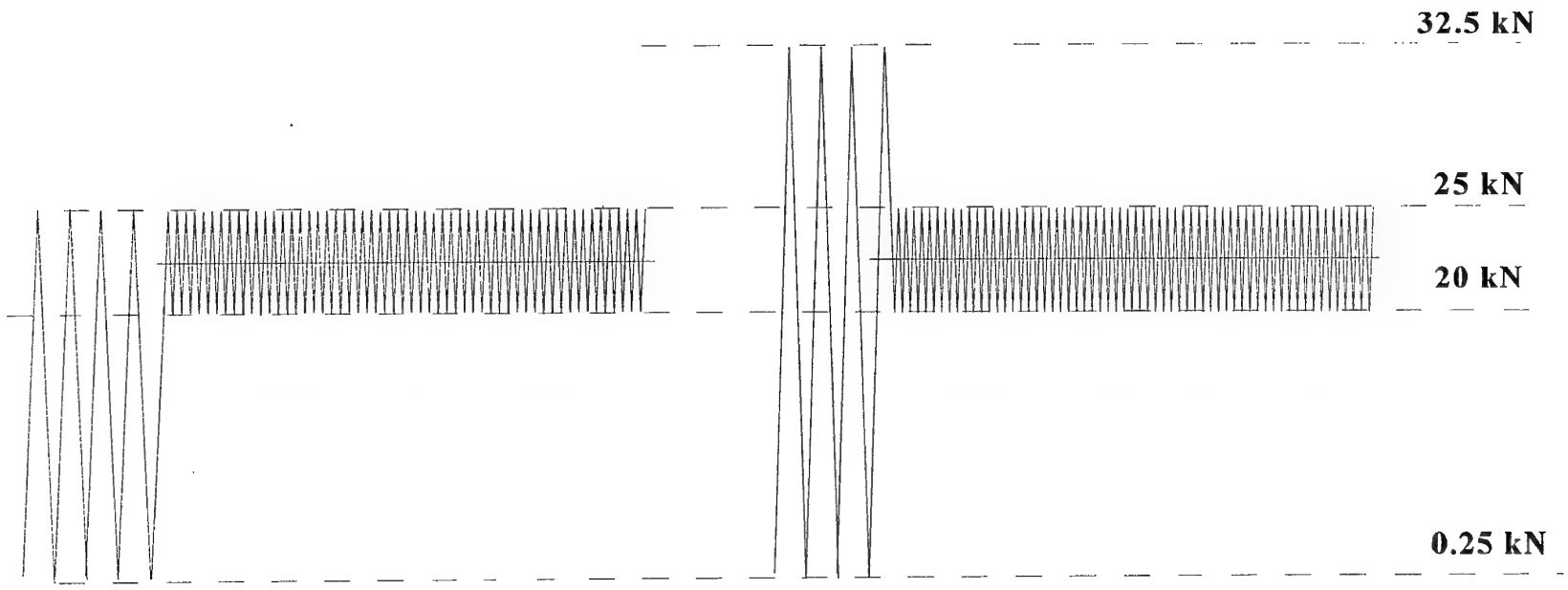

Figure 2. Schematic representation of the stress - time sequences used in the jump-in threshold tests. (a) Overload ratio, [T] = 1.0: (b) Overload ratio, [T] = 1.3.

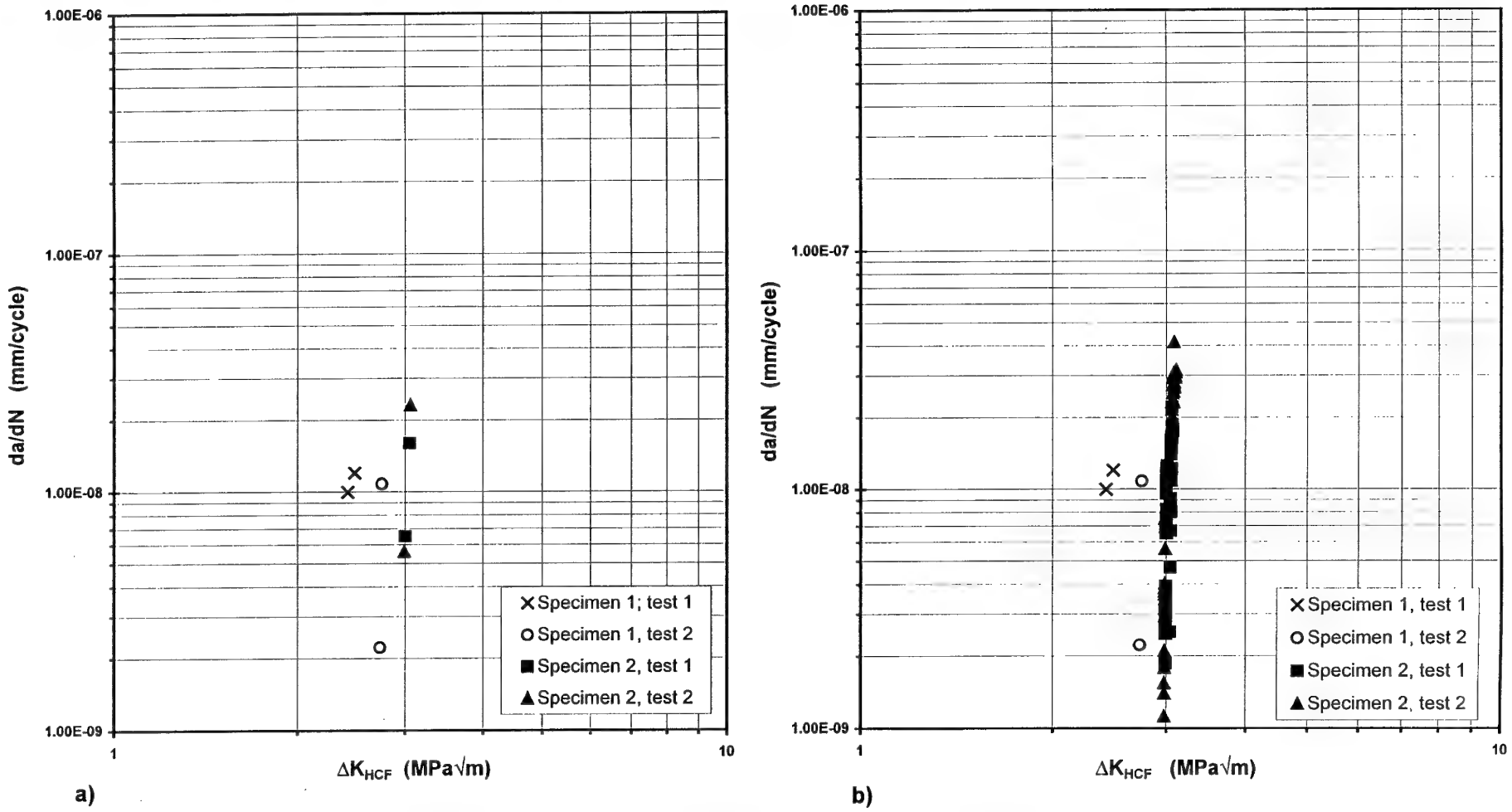

Figure 3. Comparison of methods used to represent the determination of ΔK_{th}. Data for jump-in tests at R_{HCF}=0.8. (a) Old method; (b) New method

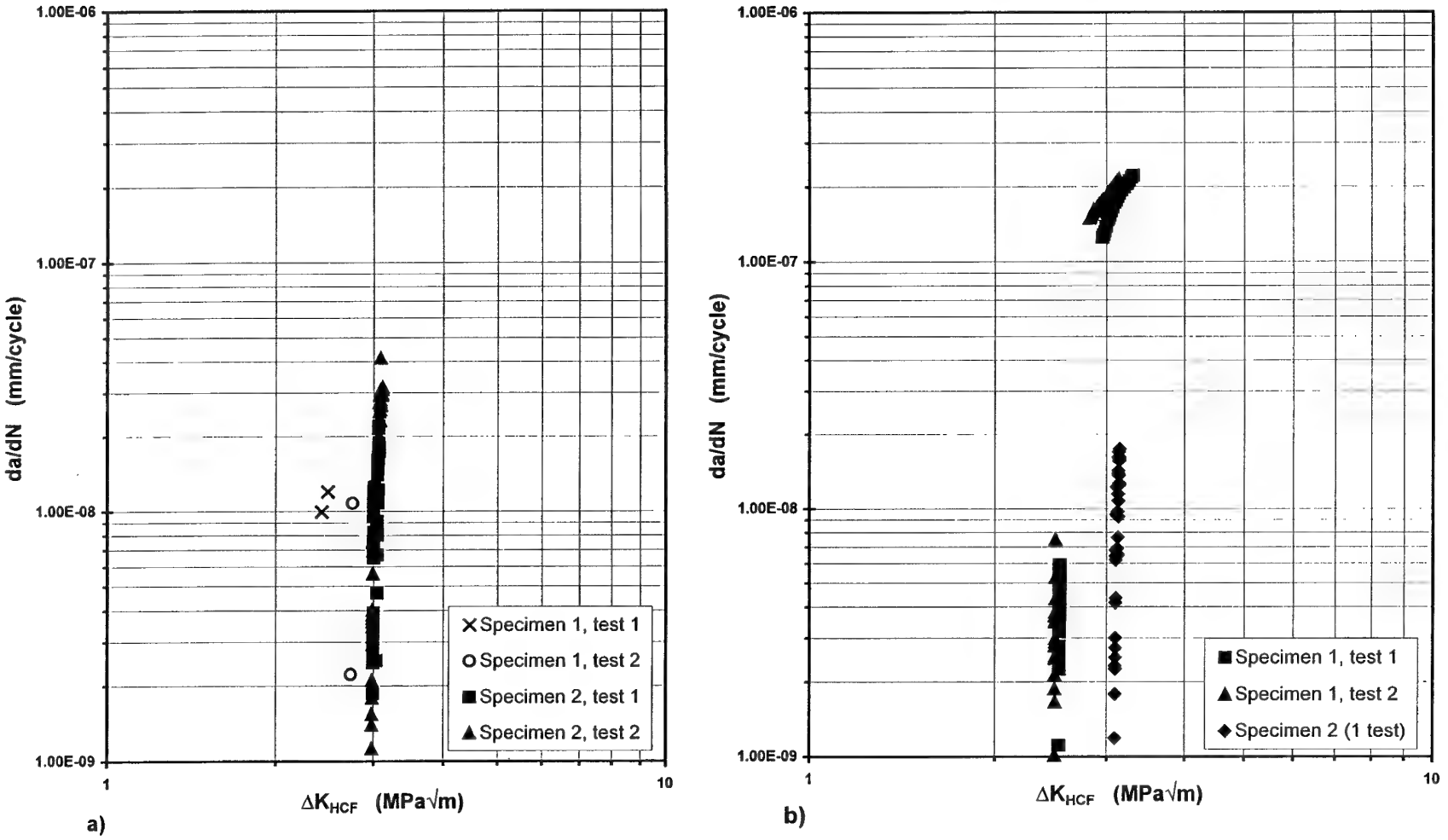

Figure 4. Comparison of FCG rates around threshold between tests at: (a) T=1.0; (b) T=1.3

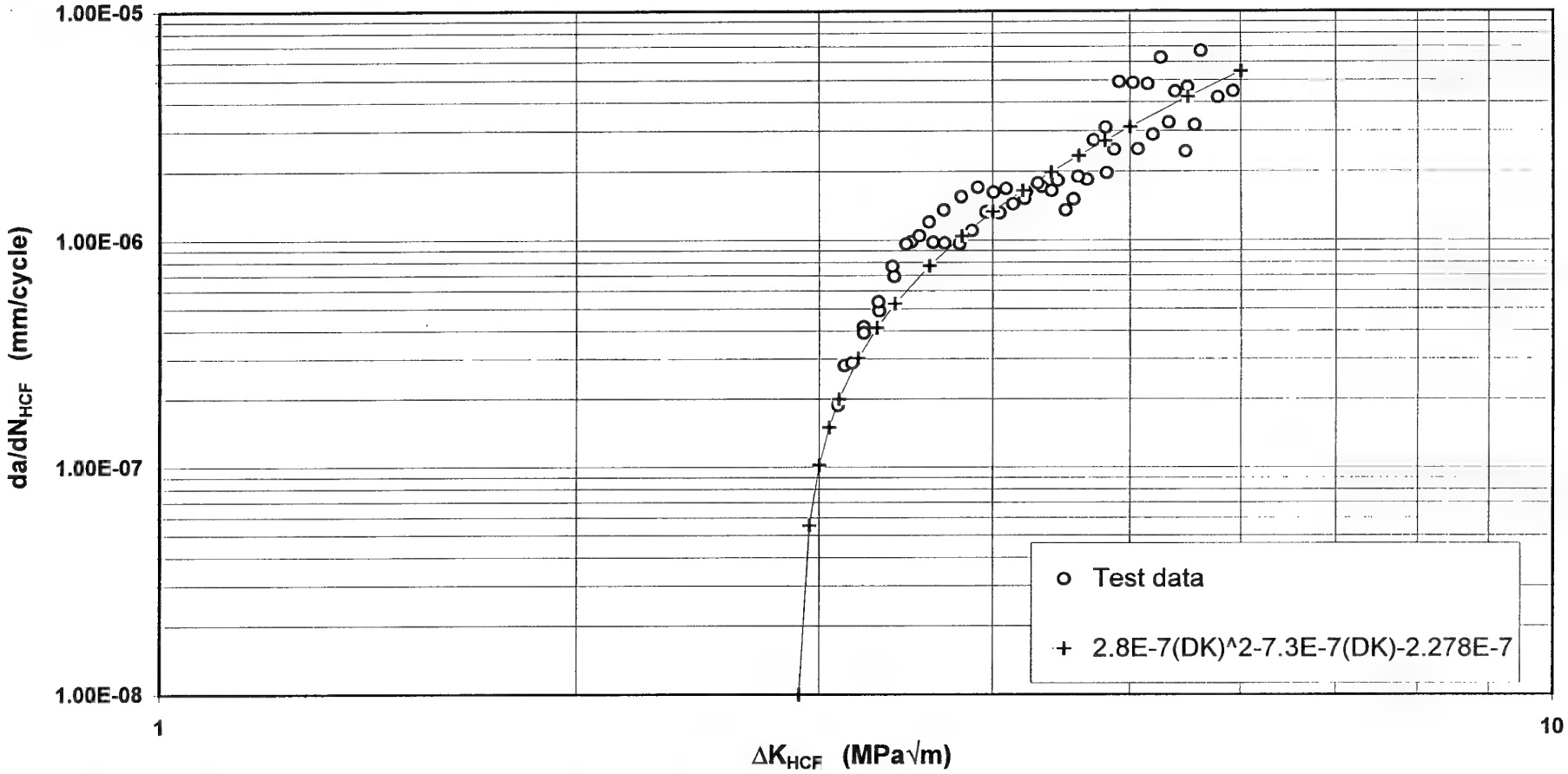

Figure 5. Near-threshold FCG rates with a visual polynomial fit through the mean of the data extrapolated to a FCG rate of 10^{-8}mm/cycle. Test data for duplicate tests at T=1.0.

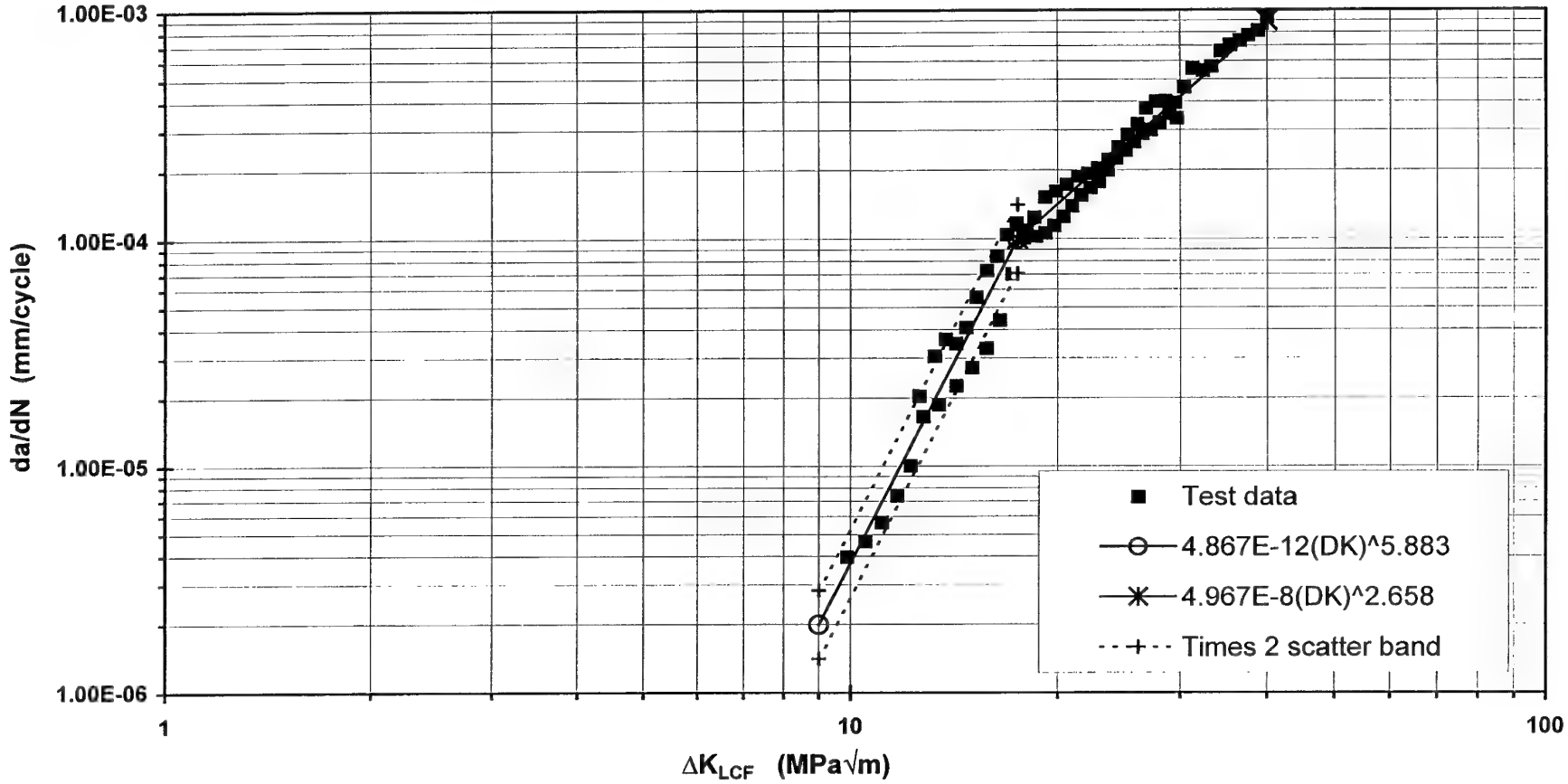

Figure 6. A bi-linear fit through the LCF only test data. The lines are used to represent LCF test data in subsequent charts. Test data for duplicate tests at R_{LCF}=0.01.

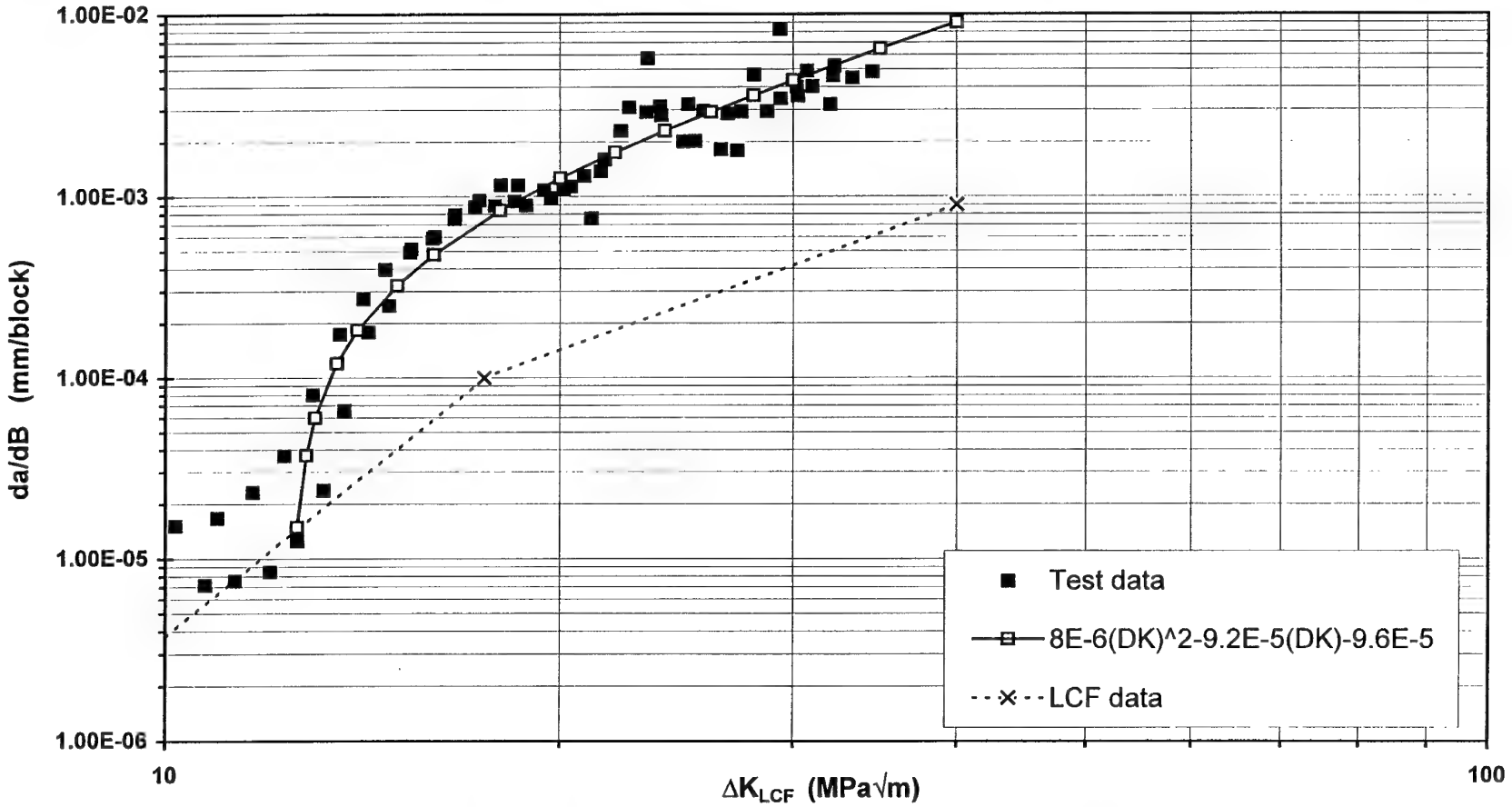

Figure 7. A polynomial fit through the FCG data for SUC tests. Test data for duplicate tests at n=1000:1.

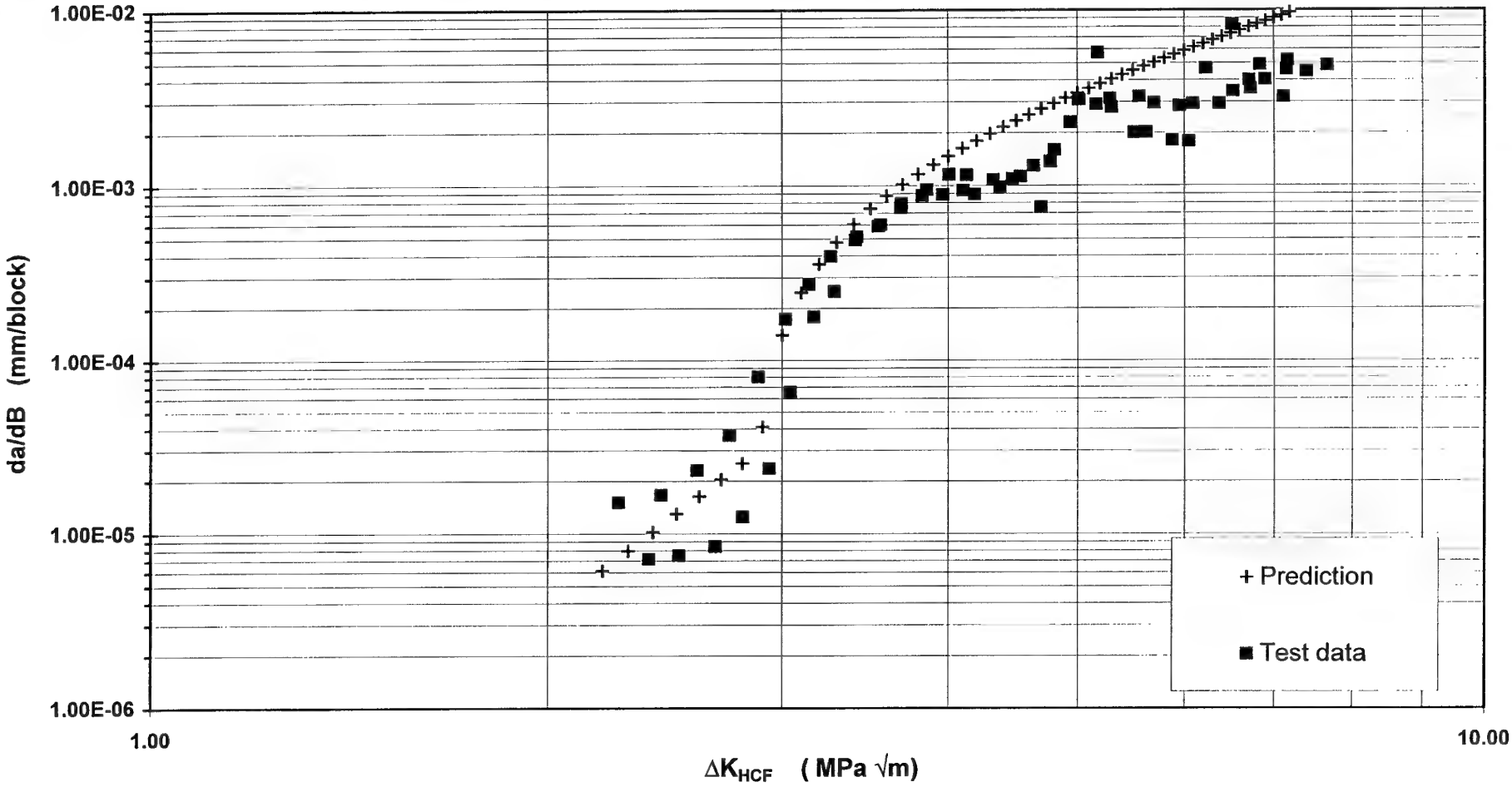

Figure 8. Comparison of predicted and experimental FCG rates for SUC tests. Test data for duplicate tests at n=1000:1.

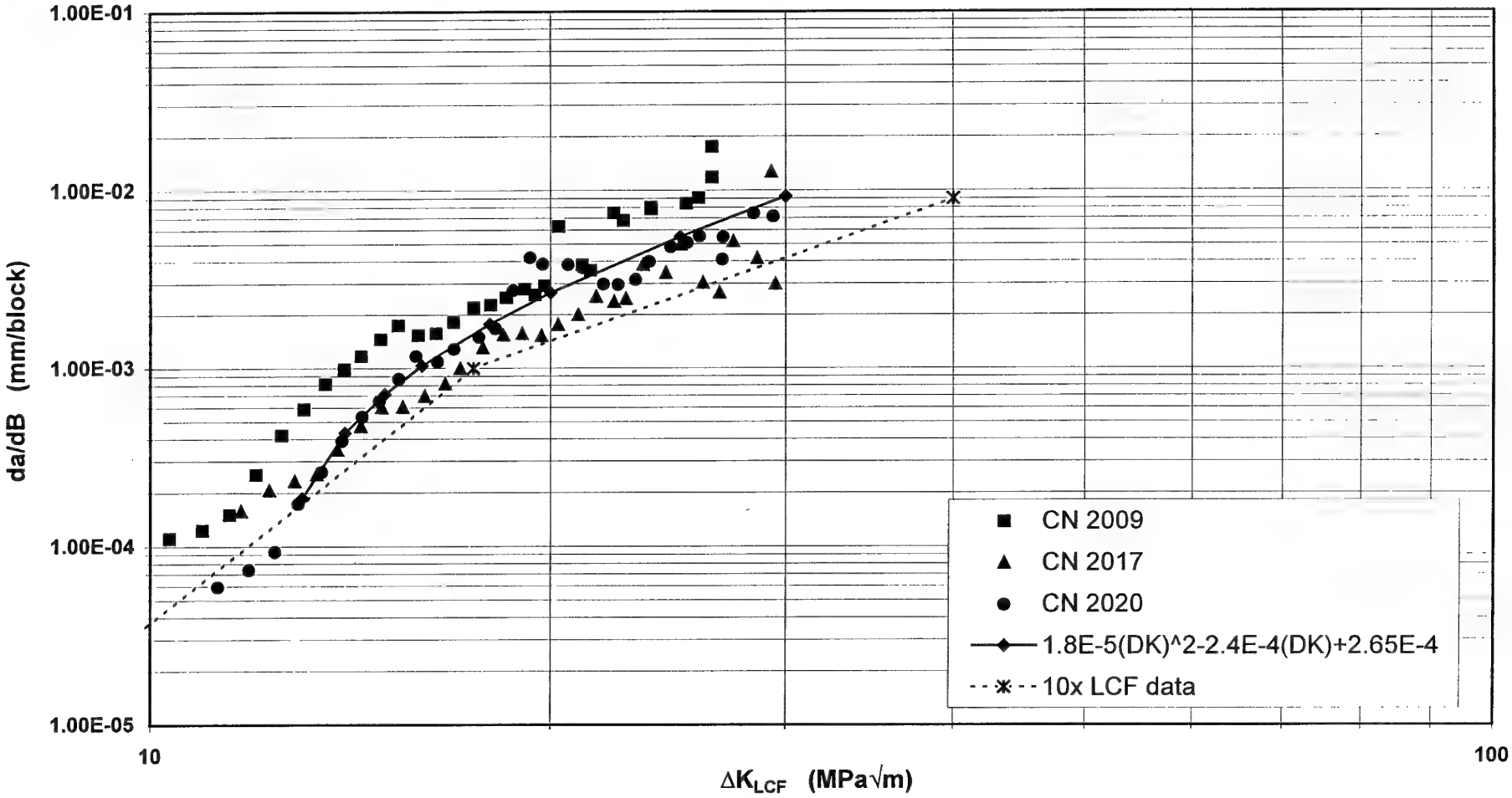

Figure 9. A polynomial fit through the FCG data for MUC tests. Test data for three tests at: T=1.0; n=1000:10.

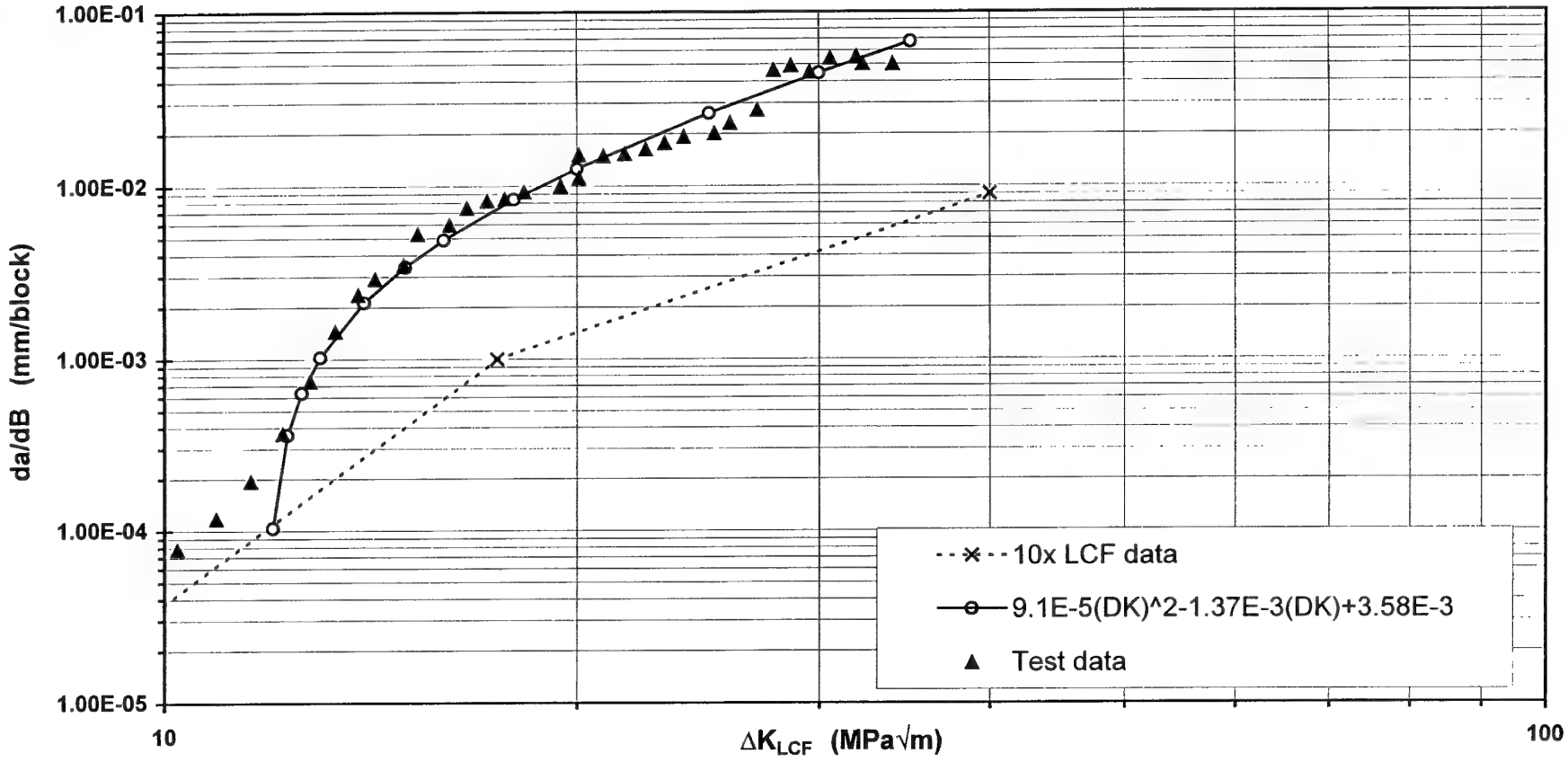

Figure 10. A polynomial fit through the FCG data for MUC tests. Test data for a single test at: T=1.0; n=10 000:10.

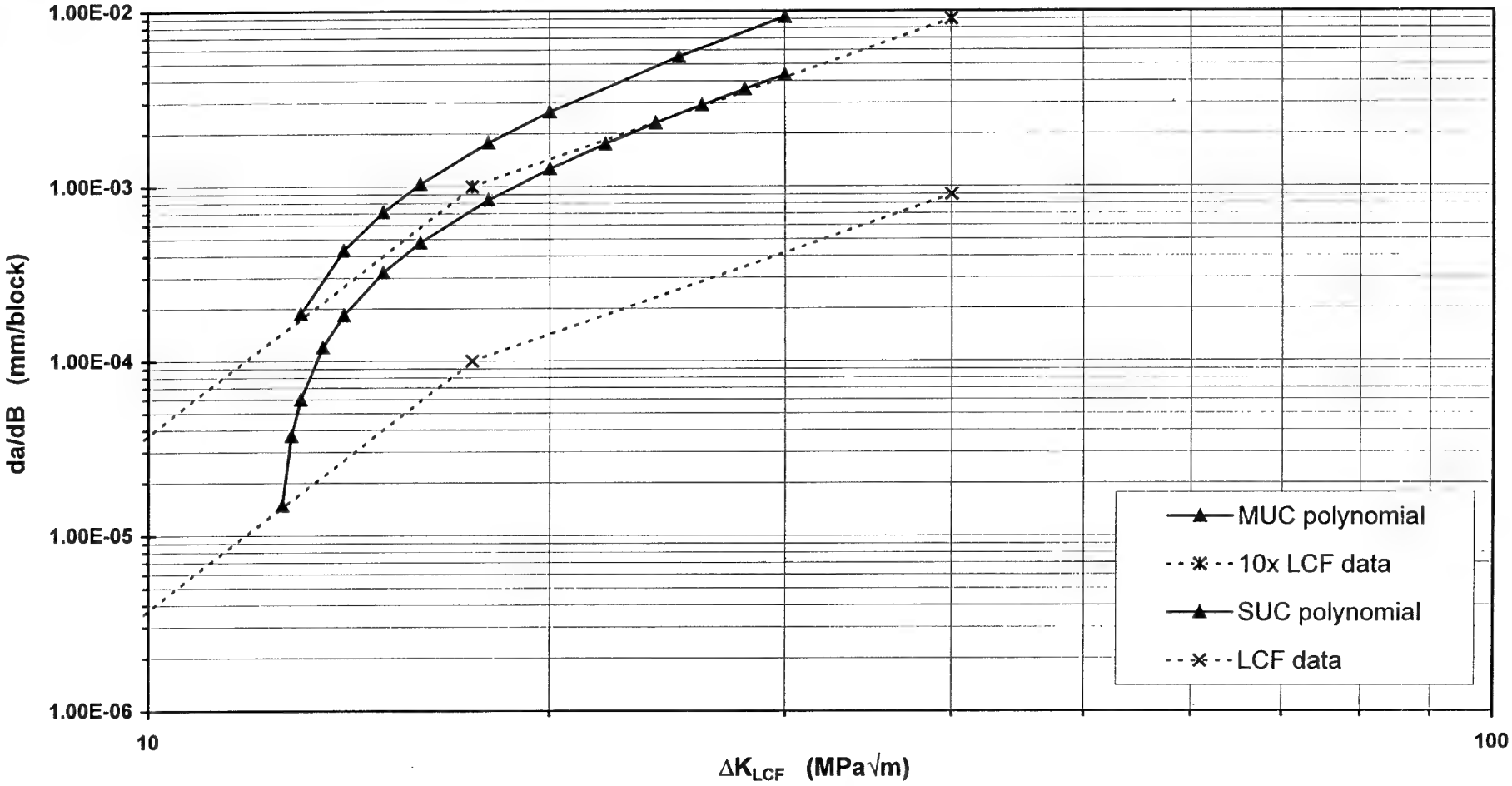

Figure 11. Comparison of FCG rates for SUC and MUC tests. Data for: T=1.0; n=1000:1 and n=1000:10.

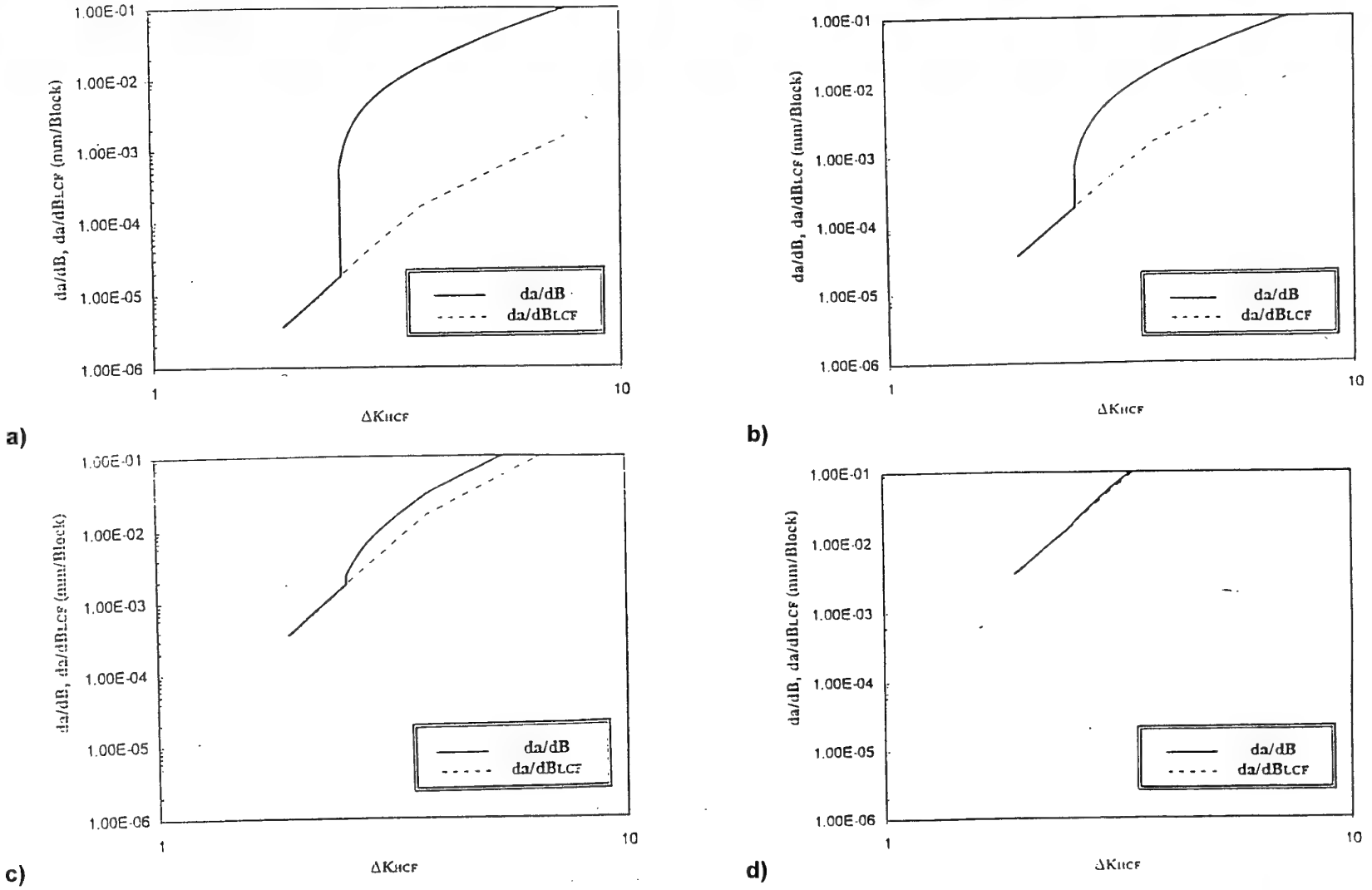

Figure 12. The predicted effect of cycle ratio on the HCF+LCF and LCF only crack growth rates. Data for: (a) n=10 000:1; (b) n=10 000:10; (c) n=10 000:100; (d) n=10 000:1000.

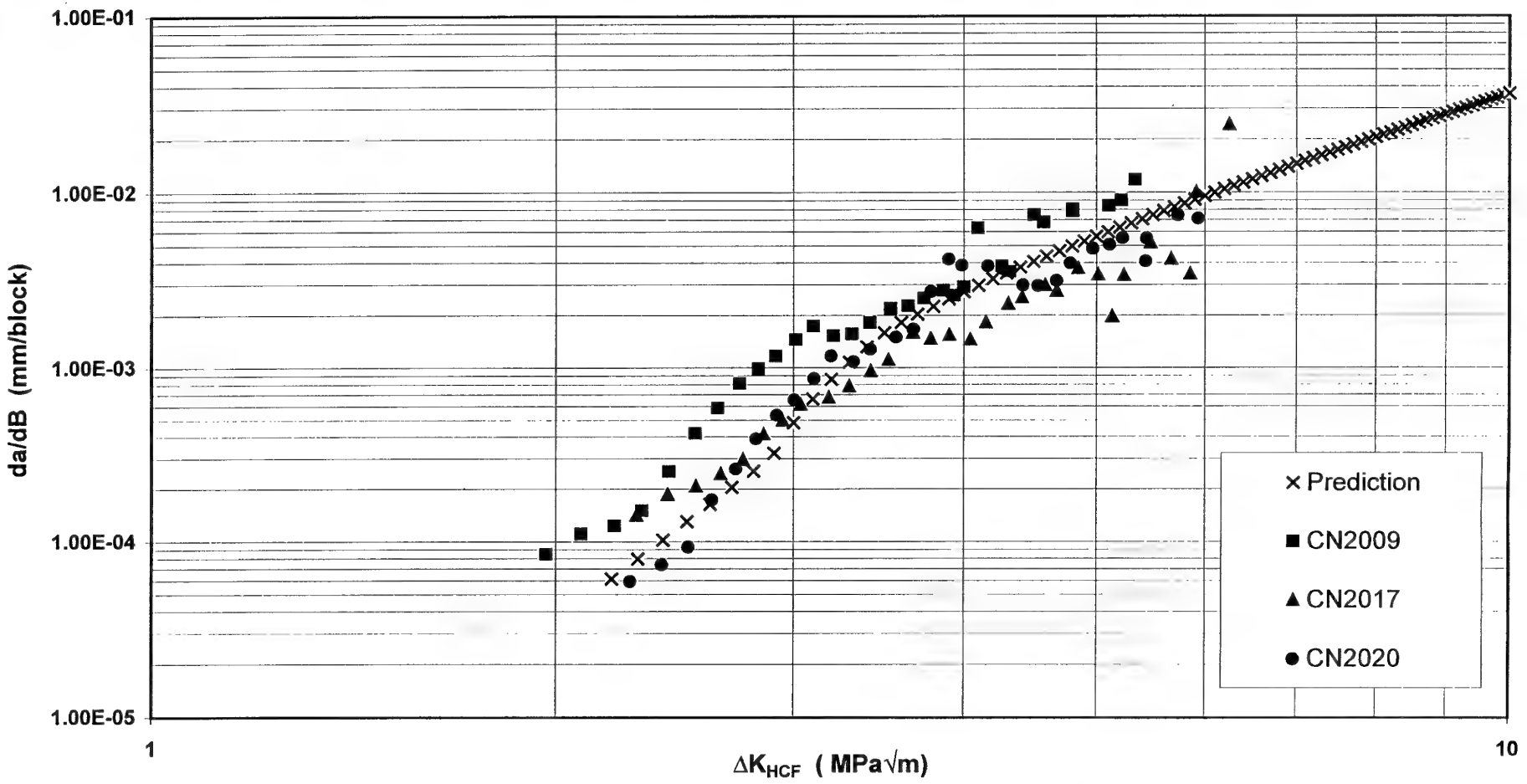

Figure 13. Comparison of predicted and experimental FCG rates for MUC tests. Test data for duplicate tests at n=1000:10.

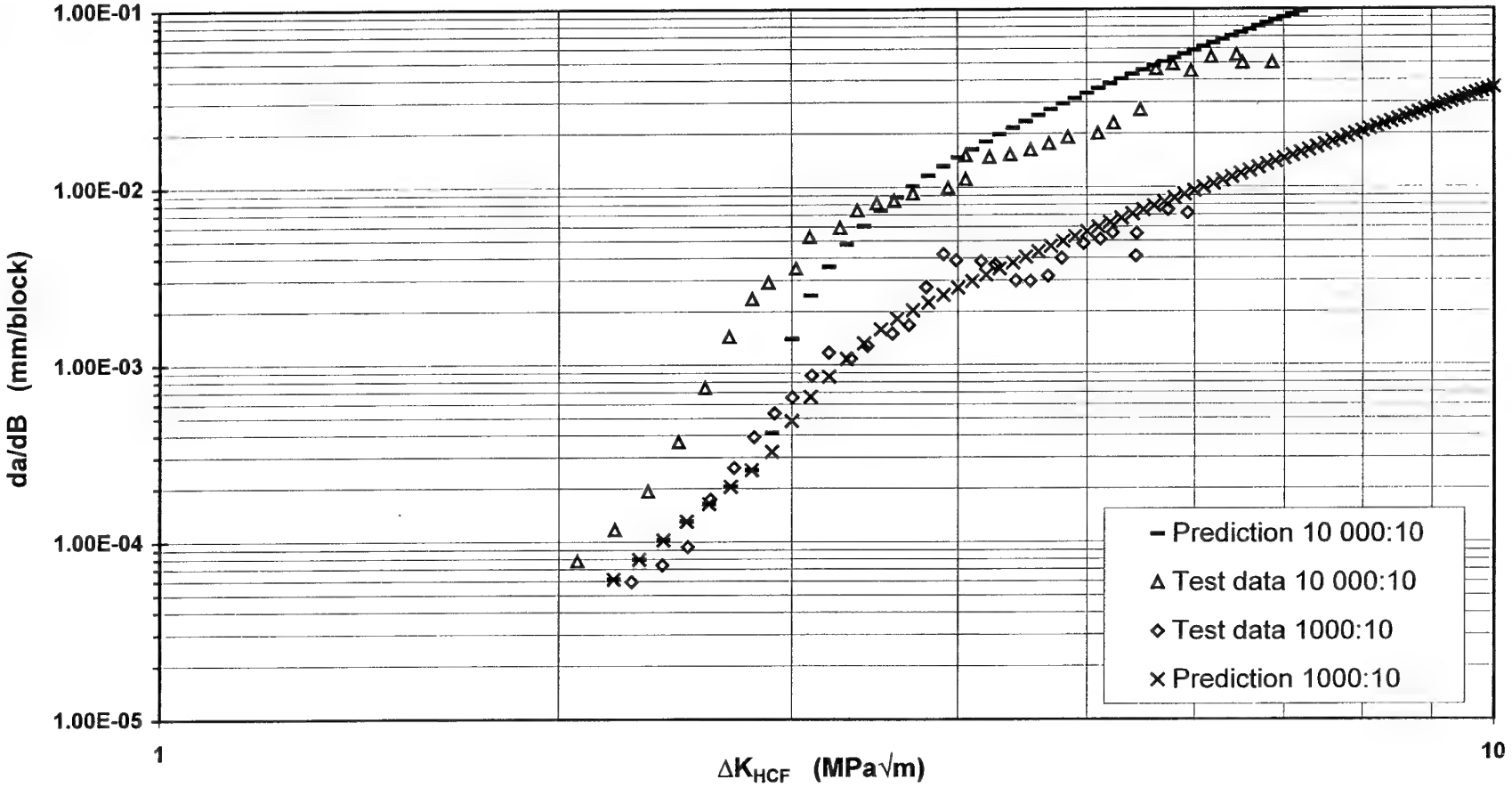

Figure 14. Comparison of predicted and experimental FCG rates for MUC tests. Test data for : T=1.0; n = 1000:10 and n = 10 000:10

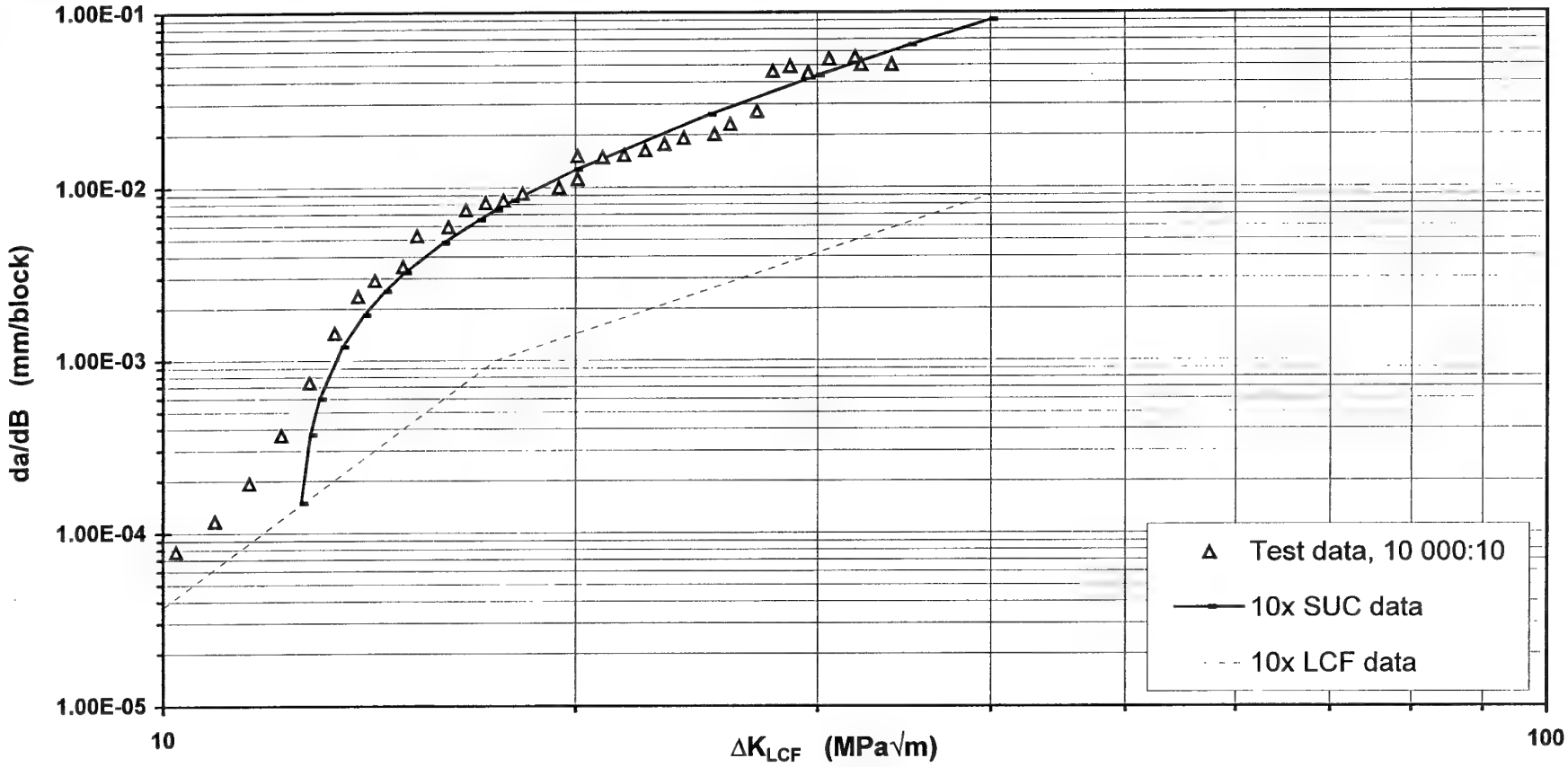

Figure 15. Comparison of FCG rate data for: a MUC test at 10 000:10, 10-times the SUC test data at 1000:1, and 10-times the LCF only test data.

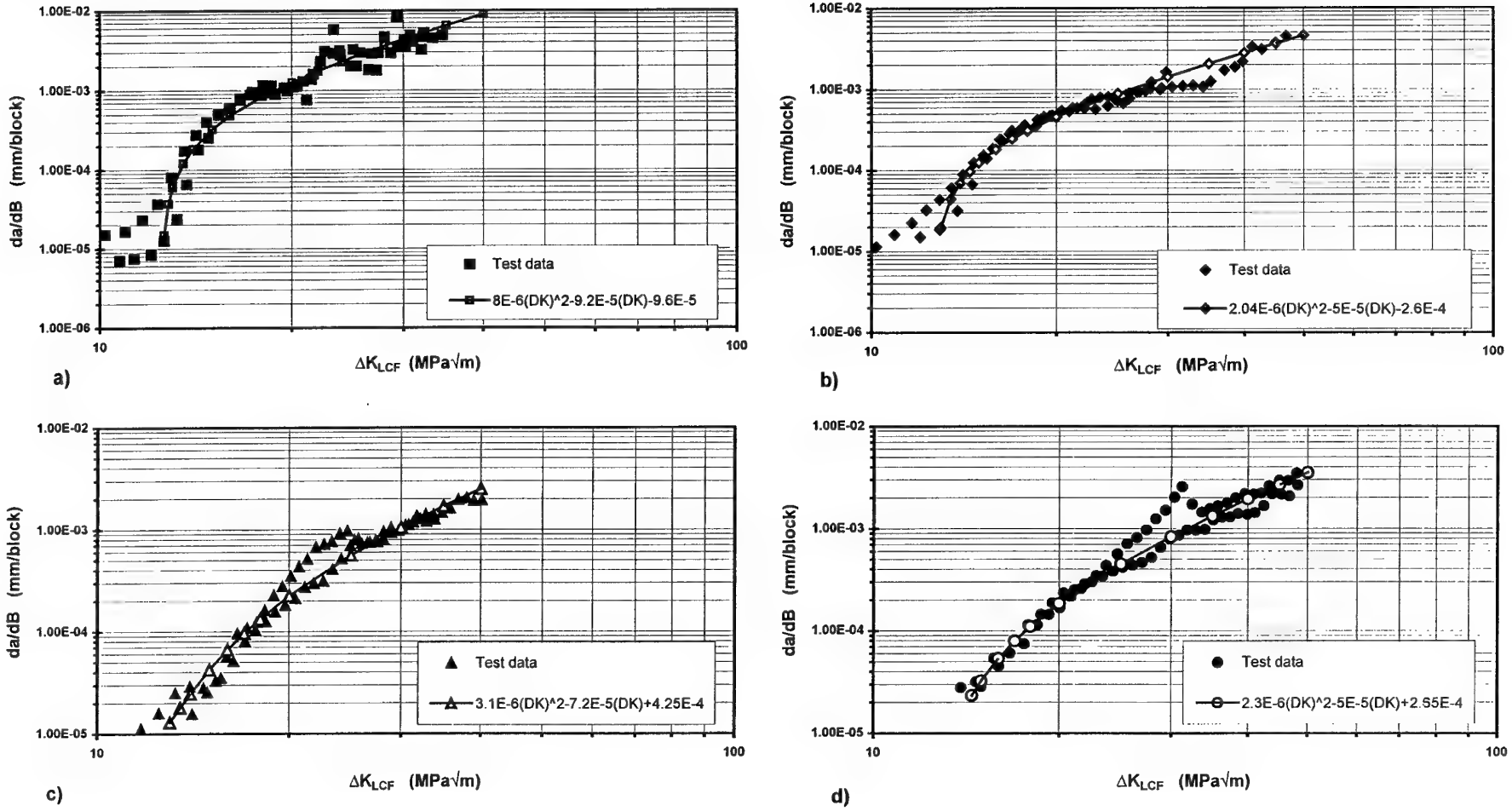

Figure 16. Polynomial fits through the FCG data for HCF+LCF tests at different overload ratios Test data for duplicate tests with n=1000:1 at: (a) T=1.0; (b) T=1.15; (c) T=1.3; (d) T=1.45.

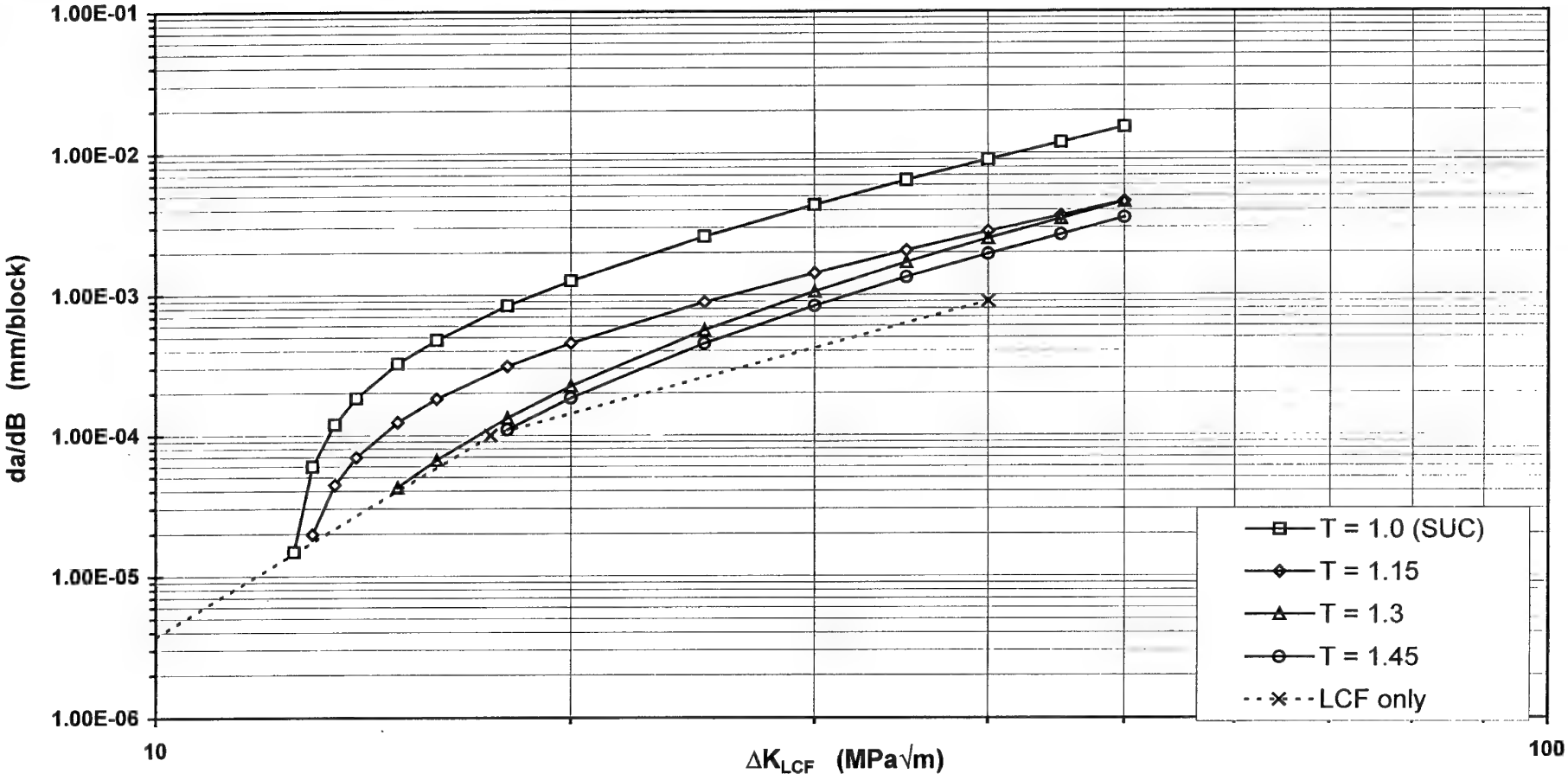

Figure 17. Comparison of the polynomial fits from Figure 16 with the LCF only test data, plotted as a factor of ΔK_{LCF}. Test data for n = 1000:1.

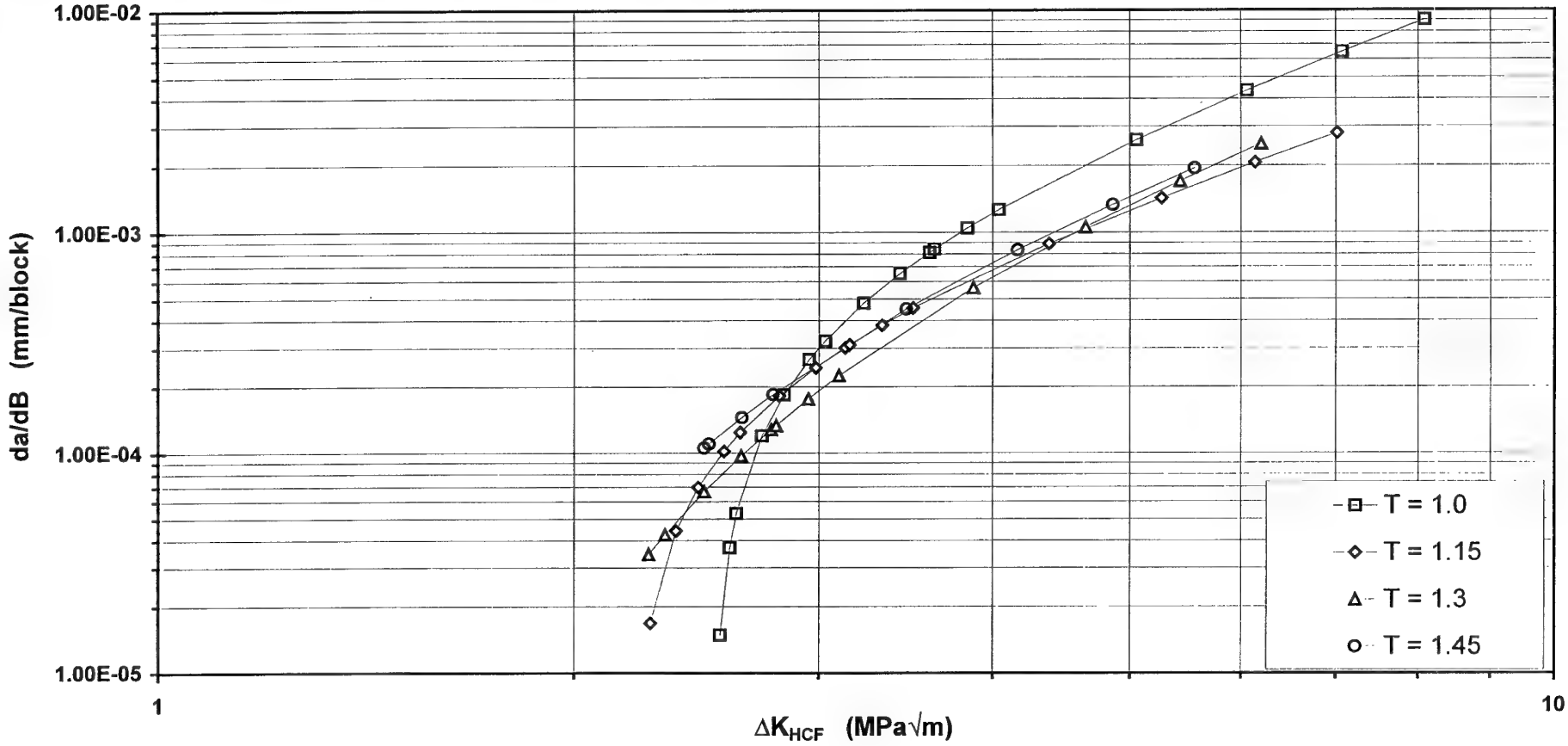

Figure 18. Comparison of the polynomial fits from Figure 16, plotted as a function of ΔK_{HCF}. Test data for n=1000:1.

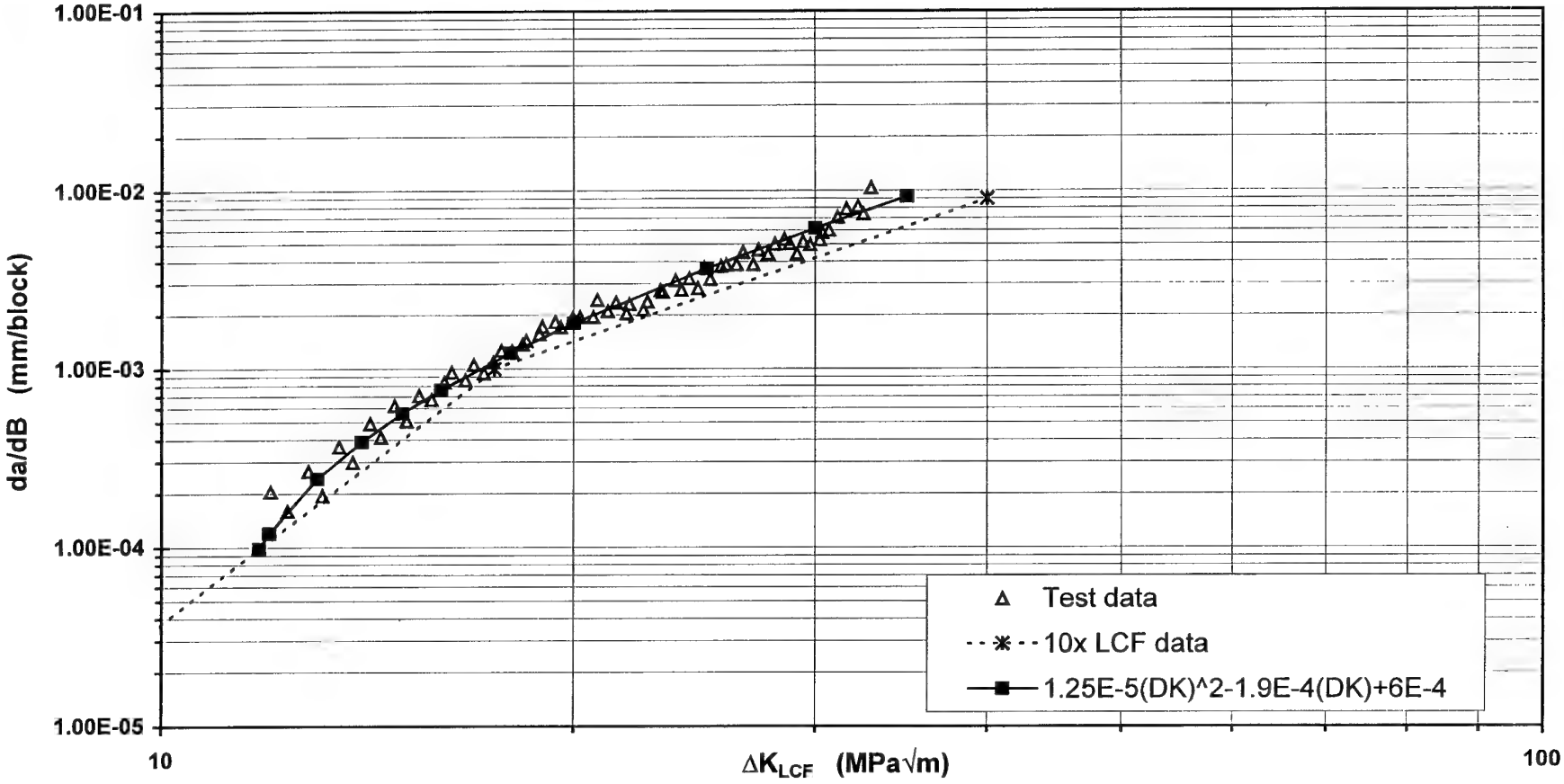

Figure 19. A polynomial fit through FCG data for MOC tests. Data for duplicate tests at: n=1000:10; T=1.3.

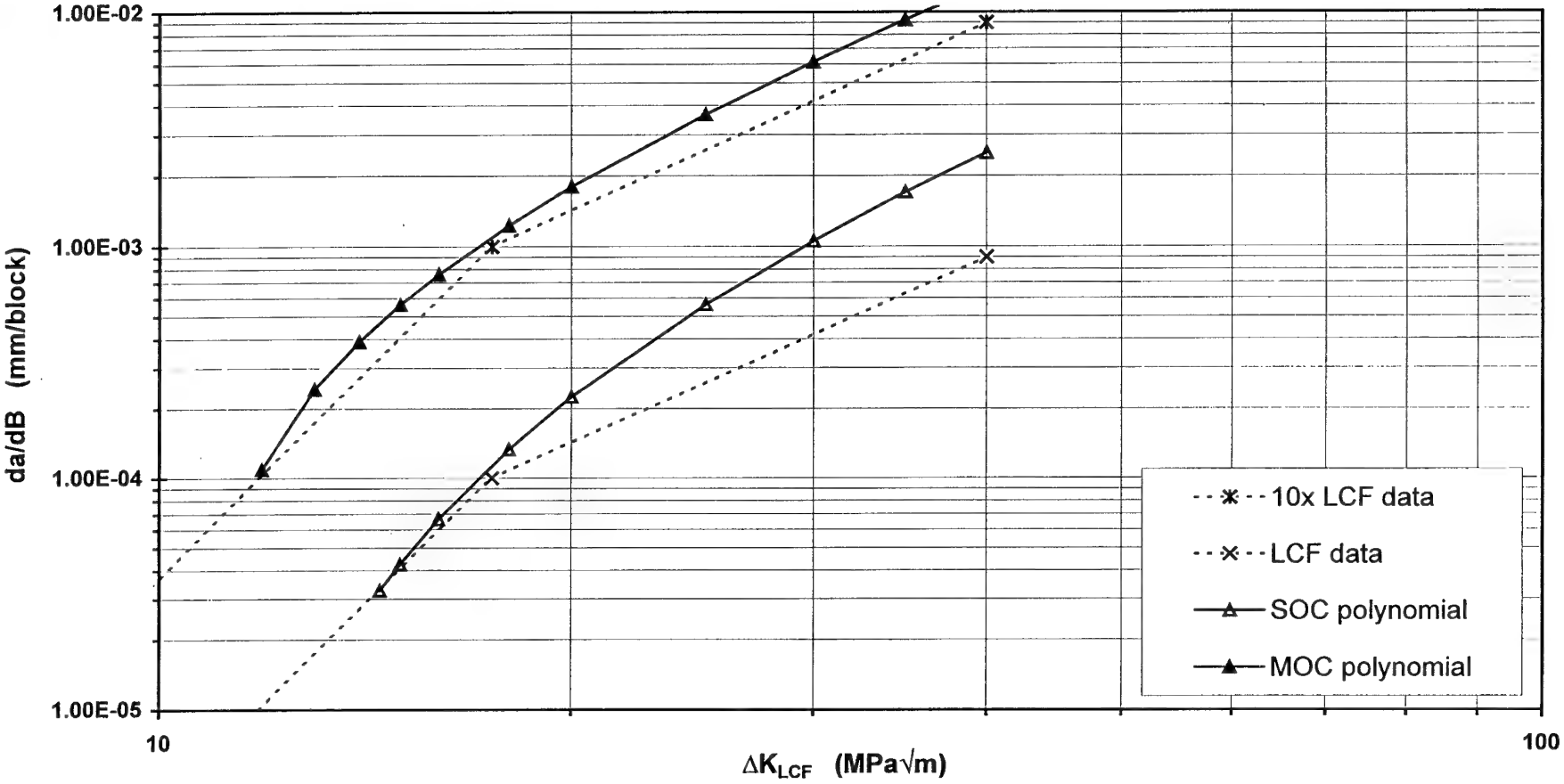

Figure 20. Comparison of FCG rates for SOC and MOC tests. Data for T=1.3 at n=1000:1 and 1000:10.

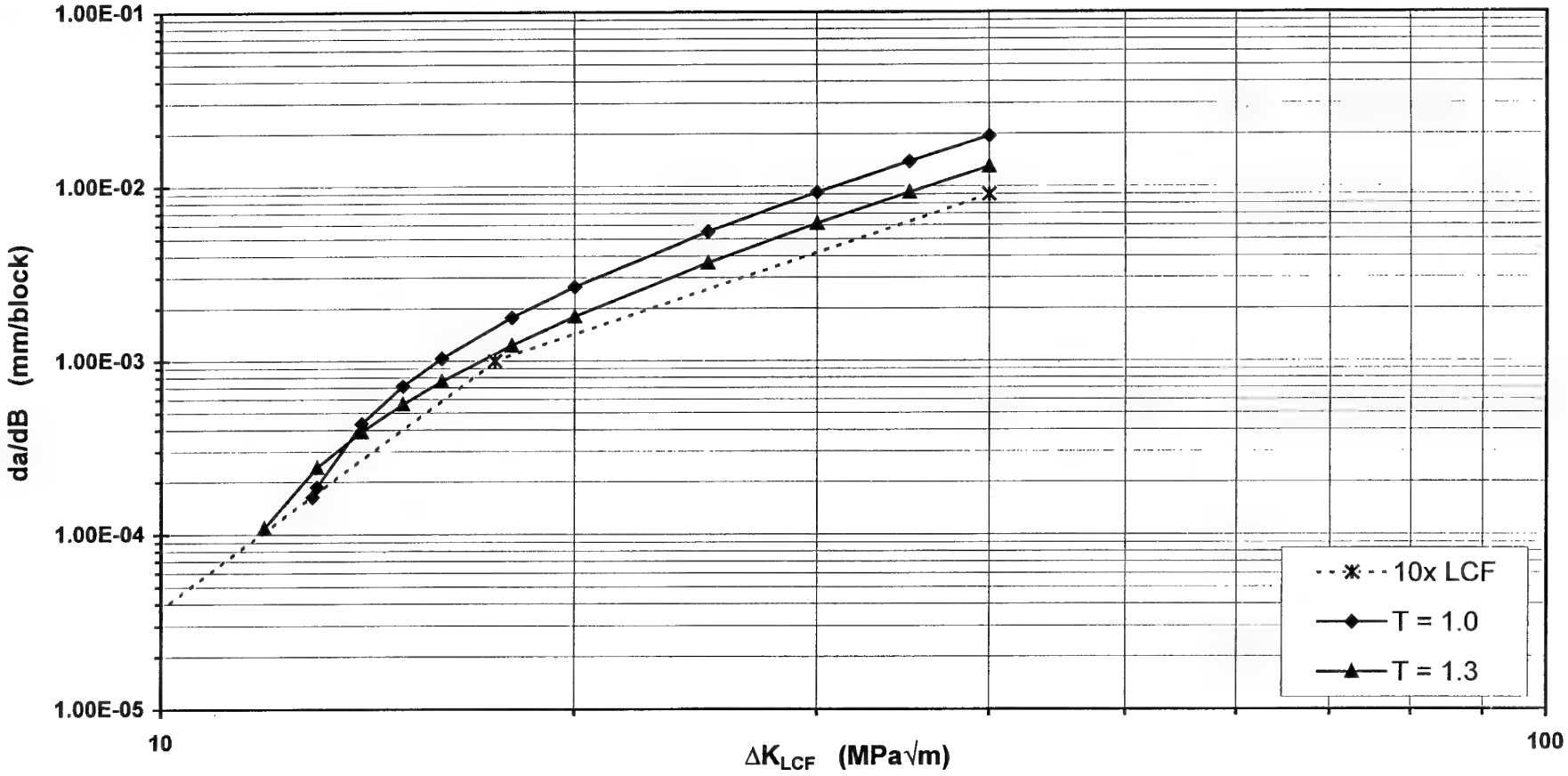

Figure 21. Comparison of FCG rates for MUC and MOC tests. Data for n=1000:10 at T=1.0 and T=1.3.

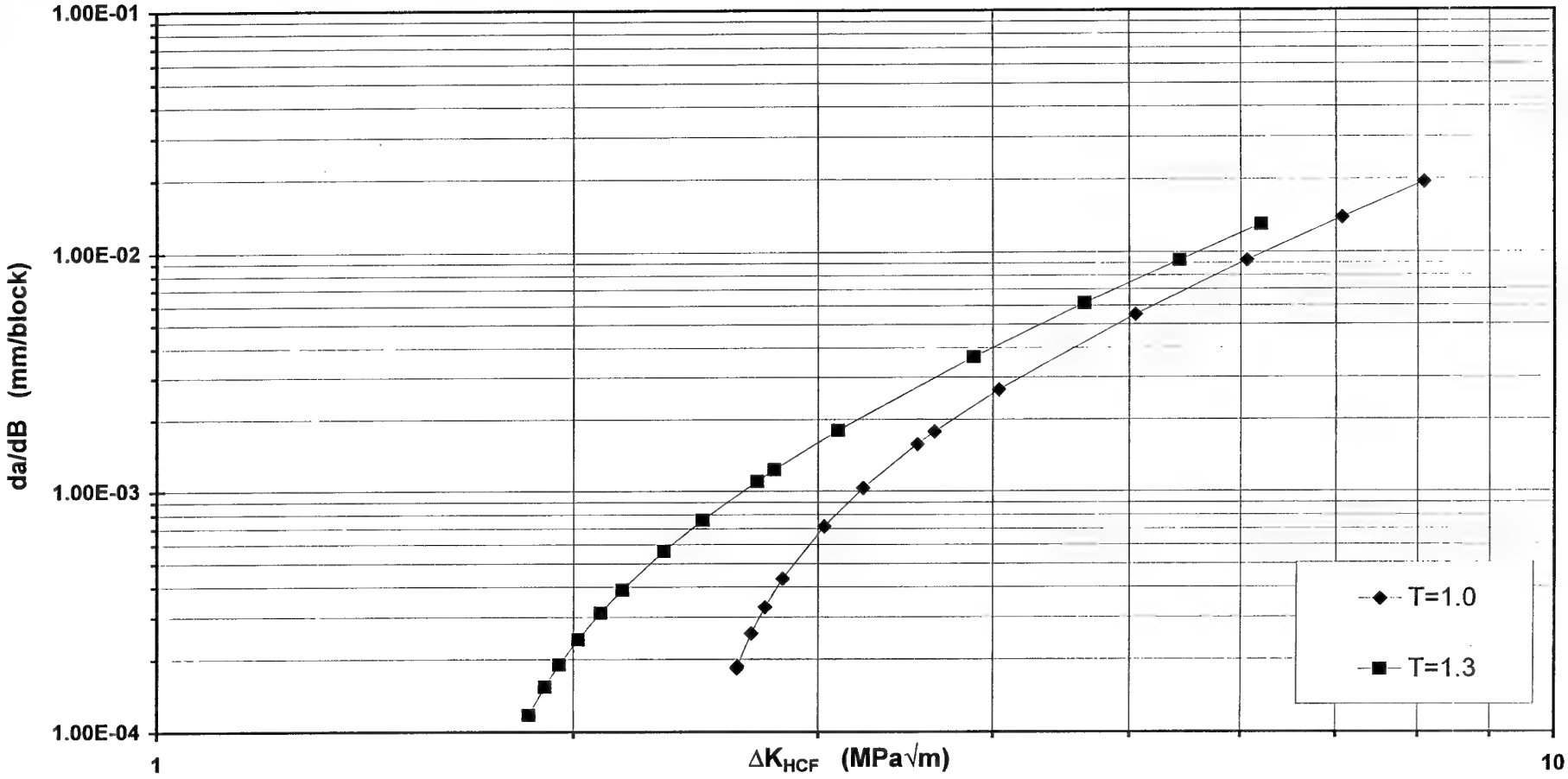

Figure 22. Comparison of the polynomial fits from MUC and MOC data, plotted as a function of ΔK_{HCF}. Data for n=1000:10 at T=1.0 and T=1.3.

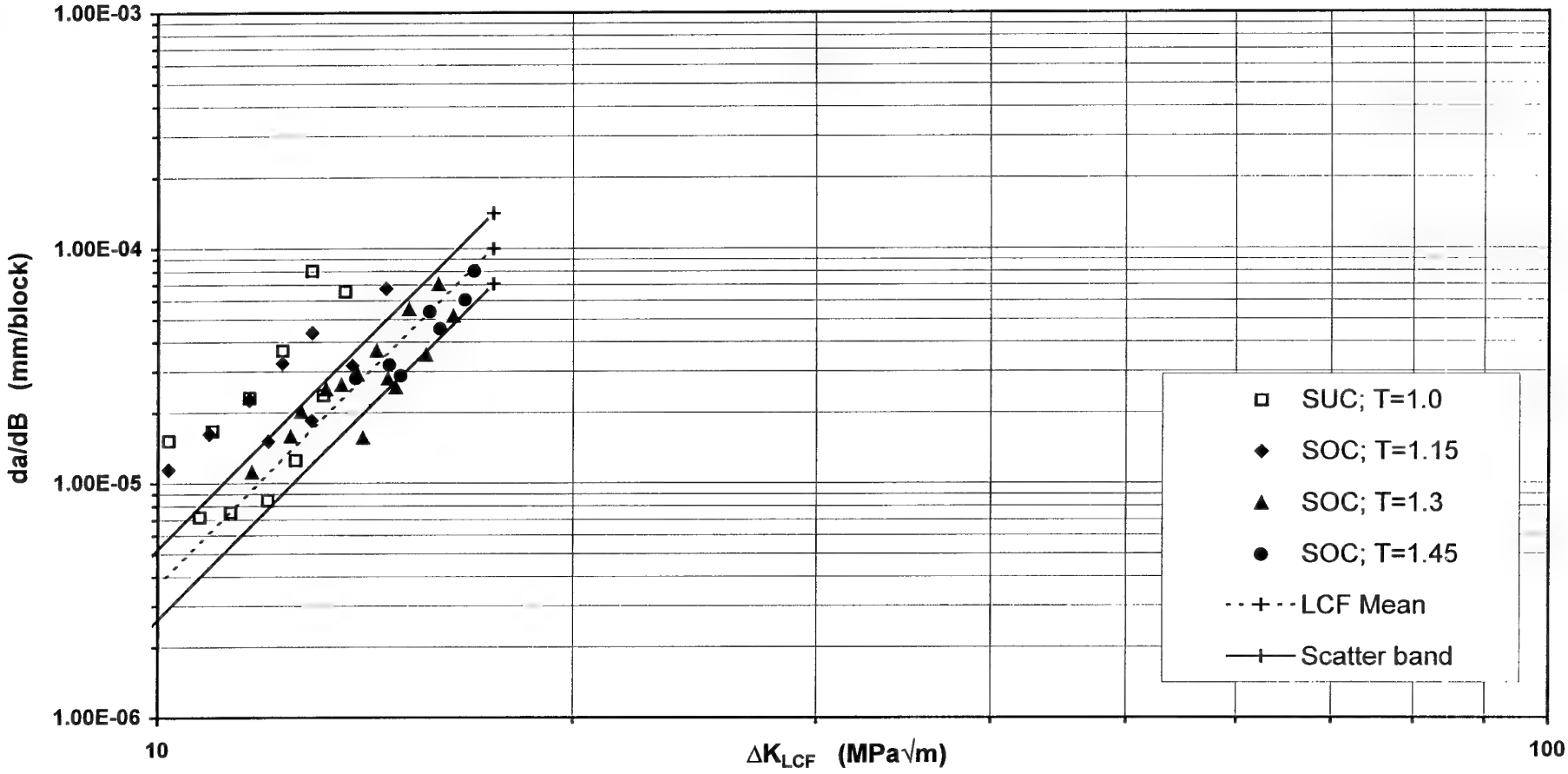

Figure 23. FCG rates for SUC and SOC test loadings relative to a LCF scatterband of times 2. Data for n=1000:1.

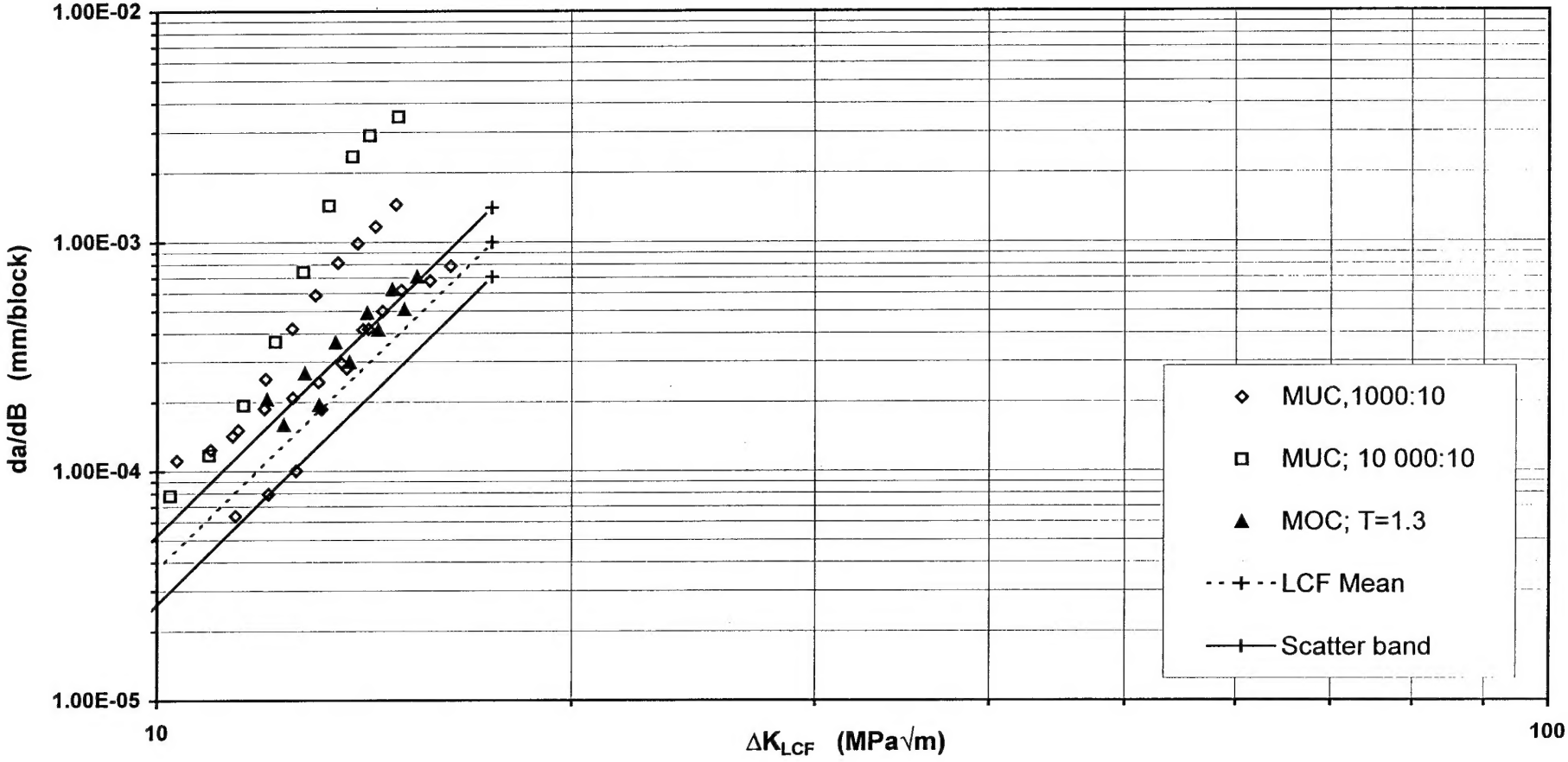

Figure 24. FCG rates for MUC and MOC test loadings relative to a LCF scatterband of times 2. Data for n=1000:1.

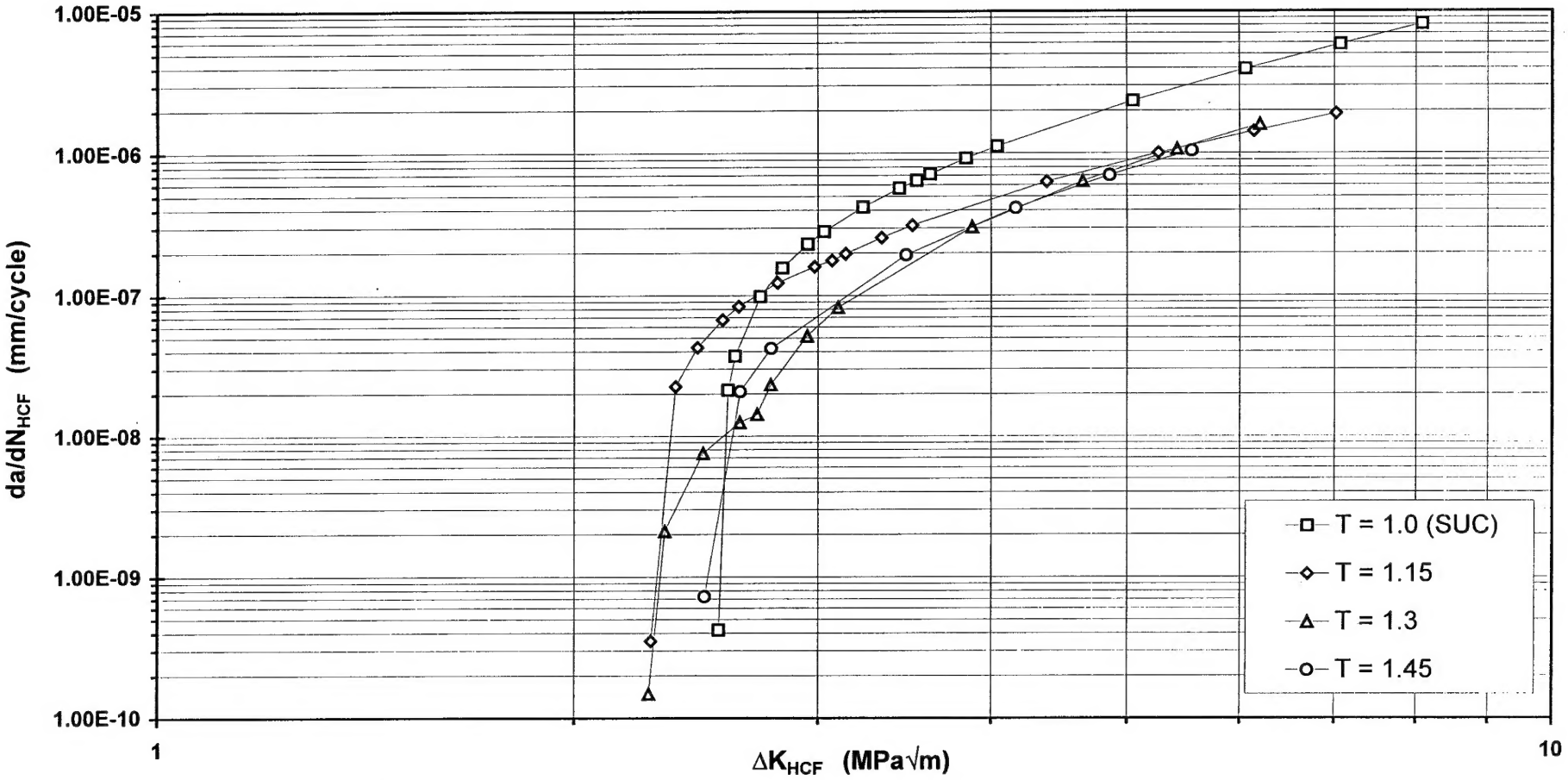

Figure 25. HCF crack growth rates calculated from SUC and SOC test data shown in Figure 16.

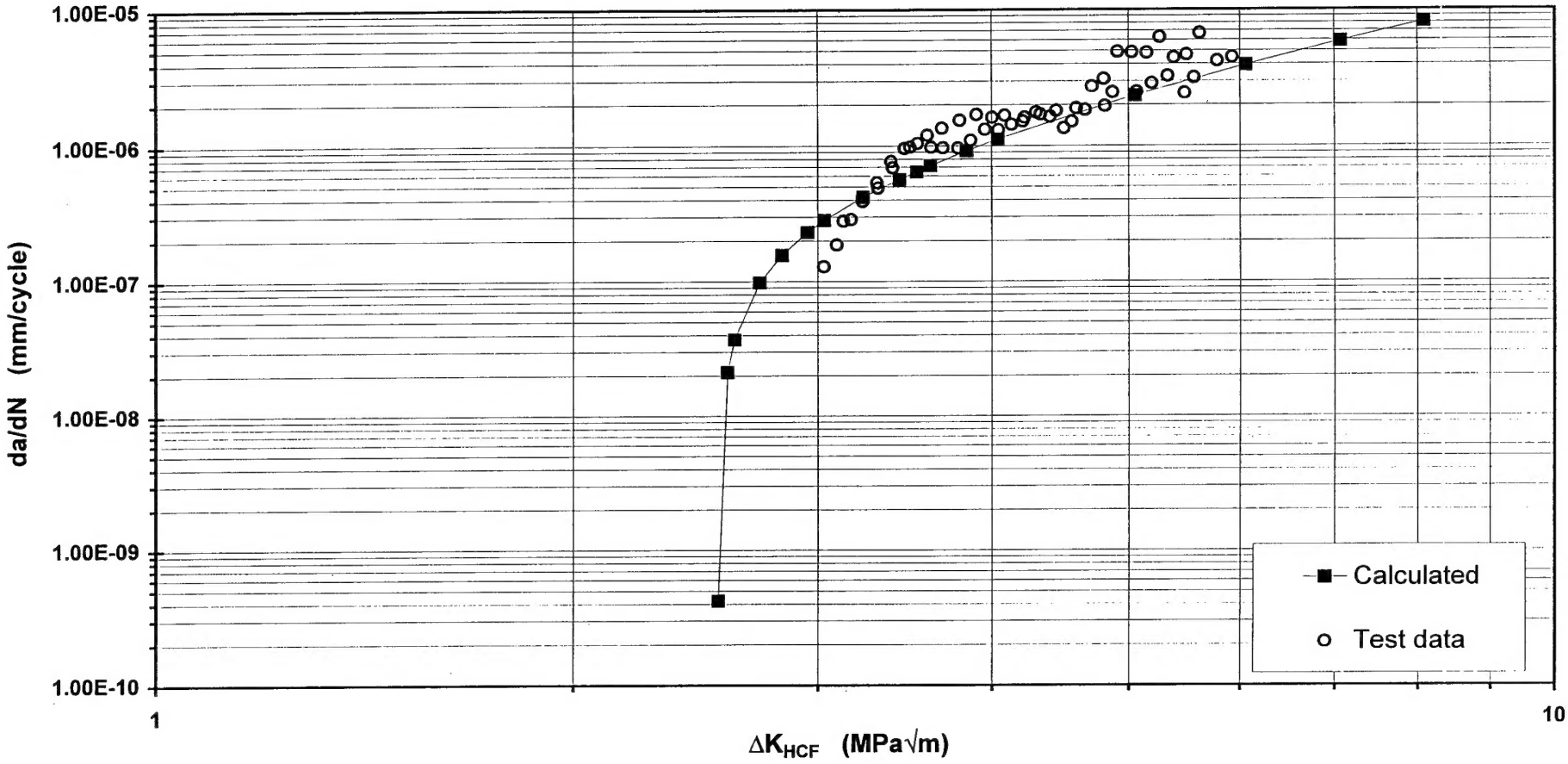

Figure 26. Comparison of experimental and calculated HCF crack growth rates. Test data for T=1.0.

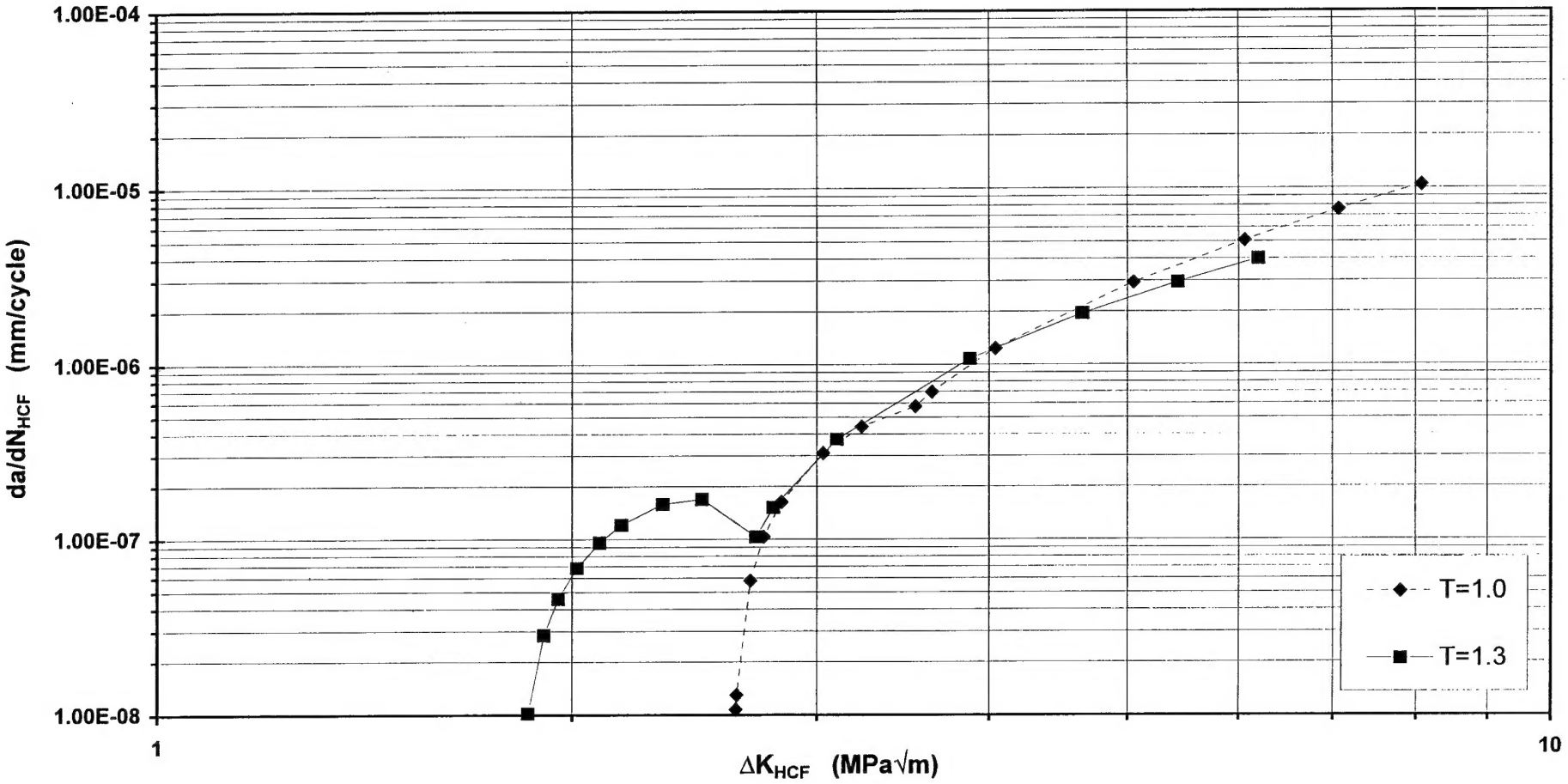

Figure 27 HCF crack growth rates calculated from MUC and MOC test data shown in Figures 9 and 19. Data for n=1000:10.